Mathematisches Forschungsinstitut Oberwolfach

Report No. 42/2009

DOI: 10.4171/OWR/2009/42

PDE and Materials

Organised by
John Ball (Oxford)
Richard D. James (Minneapolis)
Stefan Müller (Bonn)

September 13th – September 19th, 2009

Abstract. This workshop brought together mathematicians, physicists and material to discuss emerging applications of mathematics in materials science.

Mathematics Subject Classification (2000): 73xx, 35xx, 49xx.

Introduction by the Organisers

This meeting brought together an interesting and inspiring mix of mathematicians, physicists and material scientists, both theoreticians and experimentalists, to discuss new challenges for mathematics arising from materials science and the use of mathematical ideas in materials science. The talks and extensive informal discussions covered phenomena on all the relevant length scales, atomistic, mesoscopic and macroscopic, with particular emphasis and rigorous bridges between these scales.

Workshop: PDE and Materials

Table of Contents

Abstracts

The Evolution of a Crystal Surface Below the Roughening Temperature: Steps, PDE, and Self-similar Asymptotics

Robert V. Kohn
(joint work with Hala Al Hajj Shehadeh and Jonathan Weare)

Crystalline films are often grown or annealed below the roughening temperature. The microscopic physics involves attachment and detachment of atoms at steps, and diffusion of atoms across terraces. The macroscopic consequences of these mechanisms are still poorly understood. In particular, we wish to know

(a) why steps seem in many cases to self-organize, creating height profiles that are asymptotically self-similar; and
(b) whether there is a PDE that represents the large-time, large-scale behavior of a surface with many steps.

My talk addressed these questions in what is perhaps the simplest possible setting: the evolution of a monotone, one-dimensional step train separating two semi-infinite facets, in the "attachment-detachment-limited" regime [1].

The step equations. Consider N steps, located at positions $x_1, \dots, x_N$. Each step has height $1/N$; therefore the associated surface consists of $N-1$ "terraces" (of width $x_{i+1}-x_i$, $i = 1, \dots, N-1$) separating two semi-infinite "facets" at height 0 (to the left of x_1) and 1 (to the right of x_N).

There is a well-established mean-field model for the evolution of the steps. Its roots lie in the work of Burton, Cabrera, and Frank [2]; see e.g. [4] for a more recent review, and [3, 5] for treatments of one-dimensional problems similar to the one considered here. In the "attachment-detachment-limited" regime the velocity of the ith step is

$$\dot{x}_i = \mu_{i+1} - 2\mu_i + \mu_{i-1} \quad \text{where } \mu_i = (x_{i+1} - x_i)^{-3} - (x_i - x_{i-1})^{-3} \tag{1}$$

except at the extremes. At the left extreme $\dot{x}_2 = \mu_3 - 2\mu_2 + \mu_1$ and $\dot{x}_1 = \mu_2 - \mu_1$, where $\mu_1 = (x_2 - x_1)^{-3}$. At the right extreme, $\dot{x}_{N-1} = \mu_N - 2\mu_{N-1} + \mu_{N-2}$ and $\dot{x}_N = -\mu_N + \mu_{N-1}$, where $\mu_N = -(x_N - x_{N-1})^{-3}$. The physical origin of these equations will be discussed in a moment.

A convenient viewpoint. It is convenient to focus on the "slopes"

$$u_i = \frac{1/N}{x_{i+1} - x_i}, \quad \text{defined for } i = 1, \dots, N-1.$$

The step equations can then be written (by mere algebraic manipulation) as

$$\dot{u}_i = -u_i^2 \Delta_i(\Delta u^3) \quad \text{for } i = 1, \dots, N-1 \tag{2}$$

with the conventions

$$u_0 = u_N = 0 \quad \text{and} \quad (\Delta u^3)_0 = (\Delta u^3)_N = 0.$$

Here Δ_i is the finite-difference Laplacian $\Delta_i z = N^2(z_{i+1} - 2z_i + z_{i-1})$.

Physical origin of the step equations. Briefly: the step equations come from the standard Burton-Cabrera-Frank framework, using the step interaction energy $\sum \frac{1}{(x_{i+1}-x_i)^2}$ and specializing to the attachment-detachment-limited regime. In more detail: let c_i be the concentration of atoms on the terrace between x_i and x_{i+1}. Then (using the quasistatic approximation) c_i solves $D\partial_{xx}c_i = 0$ for $x_i < x < x_{i+1}$ with

$$D\partial_x c_i = k(c_i - c_i^{\text{eq}}) \text{ at } x = x_i \text{ and } -D\partial_x c_i = k(c_i - c_{i+1}^{\text{eq}}) \text{ at } x = x_{i+1}.$$

Here c_i^{eq} (the equilibrium concentration at x_i) is a constant times the first variation of the step interaction energy $\sum \frac{1}{(x_{i+1}-x_i)^2}$; D is the terrace diffusion constant; and k is a "sticking constant." The motion of each step is then governed by conservation of mass, which gives $\dot{x}_i = a\left(D\frac{\partial c_i}{\partial x}\big|_{x=x_i} - D\frac{\partial c_{i-1}}{\partial x}\big|_{x=x_i}\right)$ where $a = 1/N$ is the step height. After manipulation and nondimensionalization, one finds that the slopes $u_i = \frac{1/N}{x_{i+1}-x_i}$ solve

$$\dot{u}_i = -u_i^2\Delta_i\left[\frac{u}{1+\frac{2D}{ka}u}\Delta u^3\right] \quad \text{for } i = 1, \ldots, N-1$$

with the same conventions as above. The "attachment-detachment-limited" regime is the limiting behavior when $\frac{2D}{ka}u_i \gg 1$, i.e. when $\frac{2D}{k} \gg x_{i+1} - x_i$ for each i. In this case we recover (2) (after a suitable rescaling of time).

Steepest descent structure, estimates, and an associated PDE. One verifies that (2) represents ℓ^2-steepest descent for the functional

$$\frac{1}{6N}\sum_{i=1}^{N-1}(\Delta_i u^3)^2.$$

This makes the continuum analogue of our step law quite clear, at least formally: it is the PDE

$$u_t = -u^2\Delta\Delta(u^3) \tag{3}$$

with boundary conditions $u(0,t) = u(1,t) = 0$ and $(u^3)_{hh}(0,t) = (u^3)_{hh}(1,t) = 0$. In fact, (3) represents L^2-steepest-descent for the functional

$$\frac{1}{6}\int_0^1 (u^3)_{hh}^2\, dh$$

subject to $u(0,t) = u(1,t) = 0$. (The condition $(u^3)_{hh} = 0$ at $h = 0, 1$ is not a constraint, but rather a "natural" boundary condition.)

To prove that the step evolution law has a solution for all t, one must show that steps don't collide, and don't go to infinity in finite time. It is sufficient to show that "slopes" u_i stay positive and finite. We do this using two energy-type estimates. The first, more elementary one is:

$$\frac{d}{dt}\sum u_i^2 = -2\sum |\Delta_i(u^3)|^2 \le 0.$$

It follows that each u_i stays bounded, so the steps do not collide. The second estimate asserts that

$$\sum \left(\Delta^{-1}\frac{1}{u}\right)_i^2 \leq (At+B)^2.$$

where A and B are suitable constants, and Δ^{-1} is the inverse of the finite-difference Laplacian with a Dirichlet boundary condition. It follows that no step goes to infinity in finite time.

Our energy estimates have obvious continuum analogues. But in the continuum setting we can't conclude from these estimates that $u(h,t)$ or $u^{-1}(h,t)$ is uniformly bounded.

Asymptotic self-similarity. The profile of the evolving surface is asymptotically self-similar. In the continuous setting this means that $u(h,t) \sim t^{-1/4}\phi(h)$ for some function ϕ; in the discrete setting it means that

$$u_i(t) \sim t^{-1/4}\phi_i.$$

To prove this, we introduce "similarity variables." In the continuous case this means considering $w(h,s) = t^{1/4}u(h,t)$ where $s = \log t$; in the discrete setting it means considering

$$w_i(s) = t^{1/4}u_i(t) \quad \text{where } s = \log t.$$

Asymptotic self-similarity means that w becomes independent of s as $s \to \infty$.

Our proof is only complete for the discrete case. It rests on the observation that the equation for w is also a steepest descent; in the discrete setting it is ℓ^2 steepest descent for

$$\sum \frac{1}{6}(\Delta_i w^3)^2 - \frac{1}{8}w_i^2.$$

This functional has a unique positive critical point (in fact, it is convex when viewed as a function of w_i^3). Moreover one can show that w_i remains strictly positive and uniformly bounded as $s \to \infty$ (more energy inequalities!). It follows by a standard ODE argument that w_i is asymptotically stationary. The argument just sketched would work in the continuous setting too, if we could show that $w(h,s)$ stayed positive and bounded as $s \to \infty$.

References

[1] H. Al Hajj Shehadeh, R.V. Kohn, and J. Weare, *Step evolution for crystals of finite size: the ADL case*, in preparation.

[2] W.K. Burton, N. Cabrera, and F.C. Frank, *The growth of crystals and the equilibrium structure of their surfaces*, Philos. Trans. R. Soc. London Ser. A **243** (1951) 299–358.

[3] N. Israeli and D. Kandel, *Decay of one-dimensional surface modulations*, Phys. Rev. B **62** (2000) 13707.

[4] H.C. Jeong and E.D. Williams, *Steps on surfaces: experiment and theory*, Surf. Sci. Rep. **34** (1999) 171–294.

[5] P.W. Fok, R.R. Rosales, and D. Margetis, *Facet evolution on supported nanostructures: the effect of finite height*, Phys. Rev. B **78** (2008) 235401.

Dislocations in graphene

Michael Ortiz
(joint work with M. P. Ariza)

1. Eigendeformation theory of discrete lattice dislocations

Following [1], we regard a graphene lattice as a *cell-complex* $\mathcal{C}$, i. e., as a collection of interconnected atoms, atomic bonds and elementary areas. When regarded as members of the cell complex, we shall refer to those objects as p-cells, where p is the dimension of the cell. Thus, an atom is a 0-cell e_0, an atomic bond is a 1-cell e_1, and each of the hexagonal cells of graphene defines a 2-cell e_2. We shall denote by E_p the set of p-cells of the lattice. We recall that, by invariance under translations, the energy of a harmonic lattice can be expressed in the form [1]

$$E(u) = \frac{1}{2}\sum_{e_1\in E_1}\sum_{e_1'\in E_1} B_{ij}(e_1,e_1')du_i(e_1)du_j(e_1') \equiv \frac{1}{2}\langle Bdu, du\rangle \tag{1}$$

where $B_{ij}(e_1,e_1')$ are bondwise force constants giving the interaction energy resulting from a unit differential displacement in the jth coordinate direction at bond e_1' and a unit differential displacement in the ith coordinate direction at bond e_1 (see [4] for details). The main difference between the discrete differential representation of a harmonic lattice energy and the conventional force-constant representation is that the former exploits the invariance of the energy under translations in order to express it in terms of *bondwise force-constants* and the differential du of the displacement field. Within an *eigendeformation* framework [3], the energy of a defective lattice is assumed to take the form

$$E(u,\beta) = \frac{1}{2}\langle B(du-\beta),(du-\beta)\rangle \tag{2}$$

A straightforward calculation further reduces the energy to the form

$$E(\alpha) = \frac{1}{2}\langle B\delta\Delta^{-1}\alpha, \delta\Delta^{-1}\alpha\rangle - \frac{1}{2}\langle A^{-1}\delta B\delta\Delta^{-1}\alpha,\, \delta B\delta\Delta^{-1}\alpha\rangle \equiv \frac{1}{2}\langle \Gamma * \alpha, \alpha\rangle \tag{3}$$

where $\alpha = d\beta$ is the discrete dislocation density, Δ is the discrete Laplacian of the lattice, A is the matrix of interatomic force constants, determined by the identity $\langle Bdu, du\rangle = \langle Au, u\rangle$, and $\Gamma(l)$ is twice the interaction energy between a unit dislocation at the origin $e_2(0)$ and another unit dislocation at $e_2(l)$ and $*$ denotes discrete convolution.

2. Quadrupolar arrangement

As a validation example we consider a periodic arrangement of discrete dislocation quadrupoles of increasing size embedded in periodic cells of graphene also of increasing size. In this example, the bondwise force constants B are obtained from the harmonic model of Aizawa *et al.* [2]. The distribution of eigendeformations

$\beta_i(e_1)$ that defines one quadrupole consists of two constant and opposite Burgers vectors supported on two zig-zag chain of 1-cells, Fig. 1a. The corresponding dislocation density $\alpha_i(e_2)$ is shown in Fig. 1b.

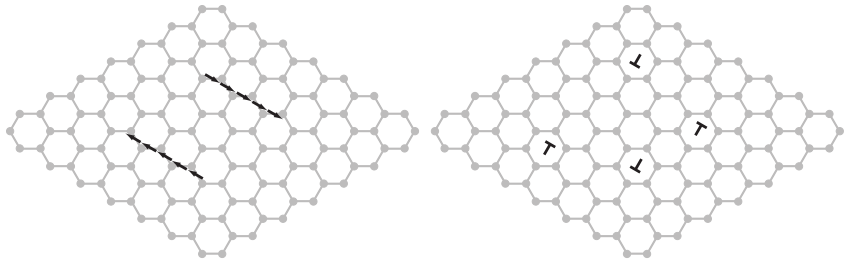

(a) (b)

FIGURE 1. Periodic quadrupolar arrangement of discrete dislocations, unit periodic cell. a) Distribution of eigendeformations $\beta_i(e_1)$ defining one quadrupole, consisting of two constant and opposite Burgers vectors over a zig-zag chain of 1-cells. b) Dislocation density $\alpha_i(e_2)$ describing the resulting quadrupole.

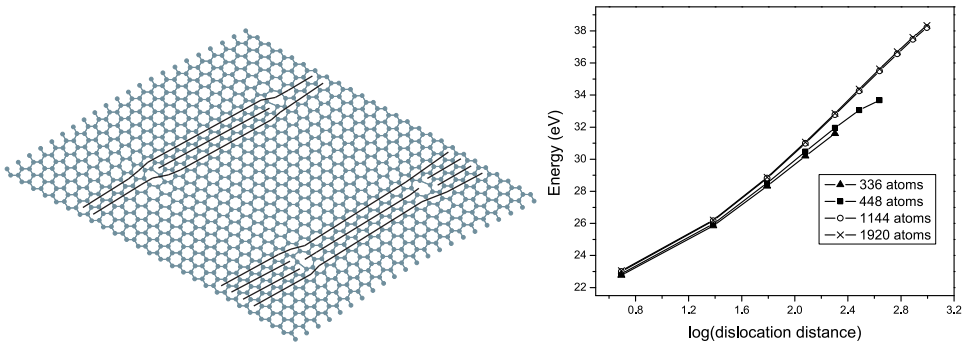

(a) (b)

FIGURE 2. a) Deformed configuration of 1144-atom periodic quadrupolar arrangement of discrete dislocations in graphene exhibiting pentagon-heptagon ring (5-7) core structures periodic. b) Energy of periodic dislocation quadrupoles in [2]-graphene as a function of dislocation separation and unit-cell size.

Deformed configuration corresponding to 1144-atom periodic cell is shown in Fig. 2a. The discrete-dislocation cores exhibit pentagon-heptagon ring (5-7) core structures consistent with the observations of Hashimoto *et al.* [5] of pairs of pentagon-heptagons attached to a missing row of atoms in a zig-zag chain in electron-beam irradiated single-walled carbon nanotube of large diameter. The energy of the periodic quadrupole arrangement per unit periodic cell, which may be regarded as an energy per dipole, is shown in Fig. 2b as a function of the dislocation separation and unit-cell size. For dislocation separations much smaller

than the cell size the energy per quadrupole is ostensibly independent of the cell size and depends on the size of the quadrupole only. Except for the smallest quadrupoles, the quadrupole energy depends logarithmically on quadrupole size, in agreement with the asymptotic analysis of Section 3.

3. Dilute limit

An appealing aspect of the eigendeformation theory of discrete lattice defects is that it lends itself to mathematical analysis within the calculus of variations. For instance, we may wish to ascertain the asymptotic behavior of the energy when a fixed dislocation mass becomes increasingly dilute. For purposes of analysis it is convenient to identify discrete dislocation distributions with functions $\alpha : \mathbb{Z}^2 \to \mathcal{A}$, obtained by representing the set E_2 of hexagonal cells as a simple Bravais lattice. Here $\mathcal{A}$ is the lattice spanned by the three Burgers vectors of graphene. The asymptotic behavior of the energy in the dilute limit is described by the following lemma (see [4] for details).

Lemma [**Dilute limit**] *Suppose that $\hat\Gamma(\theta)$ is real-valued and smooth in $[-\pi,\pi]^2\backslash\{0\}$ and $\hat\Gamma(\theta)-\hat\Gamma_0(\theta)$ is bounded in $[-\pi,\pi]^2$, where $\hat\Gamma_0(\theta)$ is the long-wavelength limit of $\hat\Gamma(\theta)$. Let $\alpha \in l^2(\mathbb{Z}^2)$ have finite energy and let α_h be the sequence of increasingly dilute dislocation densities*

$$\alpha_h(l) = \begin{cases} \alpha(l/h), & \text{if } l \in h\mathbb{Z}^2, \\ 0, & \text{otherwise,} \end{cases} \tag{4}$$

Then

$$\lim_{h\to\infty} \frac{E(\alpha_h)}{\log h} = \frac{1}{4\pi}\langle K\alpha,\alpha\rangle_{l^2(\mathbb{Z}^2)} \tag{5}$$

where

$$K = \int_{\partial[-\pi,\pi]^2} \hat\Gamma_0(\theta)\, d\theta. \tag{6}$$

is the prelogarithmic energy tensor.

In the statement of the lemma, $\hat\Gamma(\theta)$ denotes the discrete Fourier transform of $\Gamma(l)$ and $\hat\Gamma_0(\theta) = \lim_{\epsilon\to 0}\epsilon^2\hat\Gamma(\epsilon\theta)$. The proof of the lemma is a direct calculation that uses the discrete Fourier transform and the properties of weak-limits of rapidly oscillatory L^1-functions.

References

[1] M. P. Ariza and M. Ortiz, *Discrete Crystal Elasticity and Discrete Dislocations in Crystals*, Archive for Rational Mechanics and Analysis, **178** (2005), 149–226.

[2] T. Aizawa, R. Souda, S. Otani, Y. Ishizawa and C. Oshima, *Bond Softening in Monolayer Graphite Formed on Transition-Metal Carbide Surfaces*, Phys. Rev. B, **42**(18) (1990), 11469–11478.

[3] T. Mura, *Micromechanics of defects in solids*, Kluwer Academic Publishers (1987).

[4] M. P. Ariza and M. Ortiz, *Discrete Dislocations in Graphene*, Journal of the Mechanics and Physics of Solids (submitted).

[5] A. Hashimoto, K. Suenaga, A. Gloter, K. Urita and S. Iijima, *Direct evidence for atomic defects in graphene layers*, Nature **430** (2004), 870.

Instability of an elastic knot

Basile Audoly

We study the elasticity of an (open) knot tied on an infinite elastic rod, and subjected to combined tension and twist. Numerical simulation [2] and experiments with a string reveal the existence of an instability for sufficiently large applied twist. This instability leads to qualitatively different final shapes, depending on the sign of the applied moment, relative to the orientation of the knot. We present a theory for this instability in the limit of a loose knot, that is when the applied force is small enough that a loop with a radius much larger than the rod thickness is formed. This instability is related to the classical helical buckling of a straight rod, with the added twist of the presence of an imperfection (the knot). Equilibria of the knotted rod are derived analytically by means of matched asymptotic solutions of the Kirchhoff equations for elastic rods, in the range of parameters relevant to the analysis of the instability. These solutions generalize those obtained in previous work [1, 3] by including nonlinear effects in the tail.

Let α be the bending rigidity of the rod, h its thickness, T the applied tension, U the applied twist. We define the auxiliary quantities R, and $\overline{U}$ by

$$R = \sqrt{\frac{\alpha}{2\,T}}, \qquad \overline{U} = \frac{U}{\sqrt{\alpha\,T}}, \qquad \epsilon = \sqrt{\frac{h}{R}}.$$

Here, R can be interpreted as the radius of the loop for a perfectly thin rod, $\overline{U}$ is the dimensionless parameter appearing in the classical analysis of linear stability of the tails (see e. g. [4]), and ϵ is a small parameter by assumption. For an infinite, unknotted rod the threshold of linear stability is

$$\overline{U}_{\mathrm{c}} = \pm 2$$

while for a circle of radius R it is

$$\overline{U}_{\mathrm{c}}^{\mathrm{loop}} = \pm\sqrt{6}.$$

This suggests that for a *infinite*, knotted rod, the tails become unstable before the loop. As a result, a simple picture of the instability can be drawn, whereby the braided part of the knot and the loop undergo together a rigid-body motion (rotation with angle φ about the axis of symmetry and translation along this axis). Deformation of the tails is non-rigid, and can be described by a weakly non-linear analysis (see for instance [4]).

Let the parameter η measuring the proximity of the loading parameter $\overline{U}$ to threshold:

$$\eta = \sqrt{2 - |\overline{U}_{\mathrm{c}}|}. \tag{1}$$

In the limit of a loose knot, $\epsilon \to 0$, simple scaling arguments suggest that the instability takes place when

$$\eta \sim \epsilon^{1/2}.$$

A more detailed study yields an implicit relation between the rotation φ and the loading parameter η in the form

$$(\Pi_n')^2 = t^2 - \frac{t^4}{4\,s^2}, \tag{2}$$

where

$$t = \frac{\eta\,\varphi}{\epsilon}, \qquad s = \frac{2 - |\overline{U}|}{\epsilon}$$

and Π_n' is a constant depending on the knot type n, introduced in reference [3], whose value is

$$\Pi_1' = \frac{\Pi_1}{\sqrt{2}} = 1.477, \tag{3}$$

for a simple knot.

References

[1] B. Audoly, N. Clauvelin, and S. Neukirch, *Elastic knots*, Physical Review Letters **99** (2007), 164301, 2007.

[2] M. Bergou, M. Wardetzky, S. Robinson, B. Audoly, and E. Grinspun *Discrete elastic rods*, ACM Transactions on Graphics **27** (2008) 63.

[3] N. Clauvelin, B. Audoly, and S. Neukirch, *Matched asymptotic expansions for twisted elastic knots: a self-contact problem with non-trivial contact topology*, Journal of the Mechanics and Physics of Solids **57** (2009), 1623—1656.

[4] G. H. M. van der Heijden and J. M. T. Thompson., *Helical and localised buckling in twisted rods: A unified analysis of the symmetric case*, Nonlinear Dynamics **21** (2000), 71–99.

Mechanical stabilization of single crystals of shape memory alloys: Open questions

Hanuš Seiner

(joint work with Michal Landa and Ondřej Glatz)

The shape memory materials are able to undergo fully reversible (thermoelastic) martensitic transitions between high–temperature, highly symmetric phase (austenite) and low–temperature phase (martensite) with lower crystallographic symmetry. The theoretical description of these transitions can be done within the frame of continuum mechanics [1, 2], representing individual phases coming into play by deformation gradients and the compatible interfaces between them by rank-1 connections. This description is sufficient for qualitative explanation of the effect of *mechanical stabilization of martensite* [3], which is a phenomenon occurring in single crystals of the shape memory alloys. Due to this effect, the reverse transition from martensite to austenite (the shape recovery process) does not start at any given transition temperature. Instead, the critical temperature for this transition depends on the initial martensitic microstructure and possibly also on the dimensions or the shape of the specimen. Detailed and quantitative analysis of this phenomenon is still missing, as far as both the experimental observations and mathematical modeling are concerned. The stabilization itself rises

a plenty of interesting (from the thermodynamical point of view) and still open questions, originating from the multiscale character of the problem (see Fig.1). For example: Is there any understandable relation between the temperature shift and the initial martensitic microstructure? Which thermodynamic principles govern the formation and propagation of the interfacial microstructures (microstructural objects enabling compatible connection between the initial martensitic microstructure and austenite, [4])? What is the mechanism of nucleation of austenite in the stabilized martensitic microstructure? Is it possible to obtain a *fully stabilized marteniste*, i.e. to tune the microstructure, the crystallographic orientation and the dimensions of the specimen such that the austenite phase cannot nucleate at all (i.e. to shift the critical temperature e.g. above the melting point of martensite)?

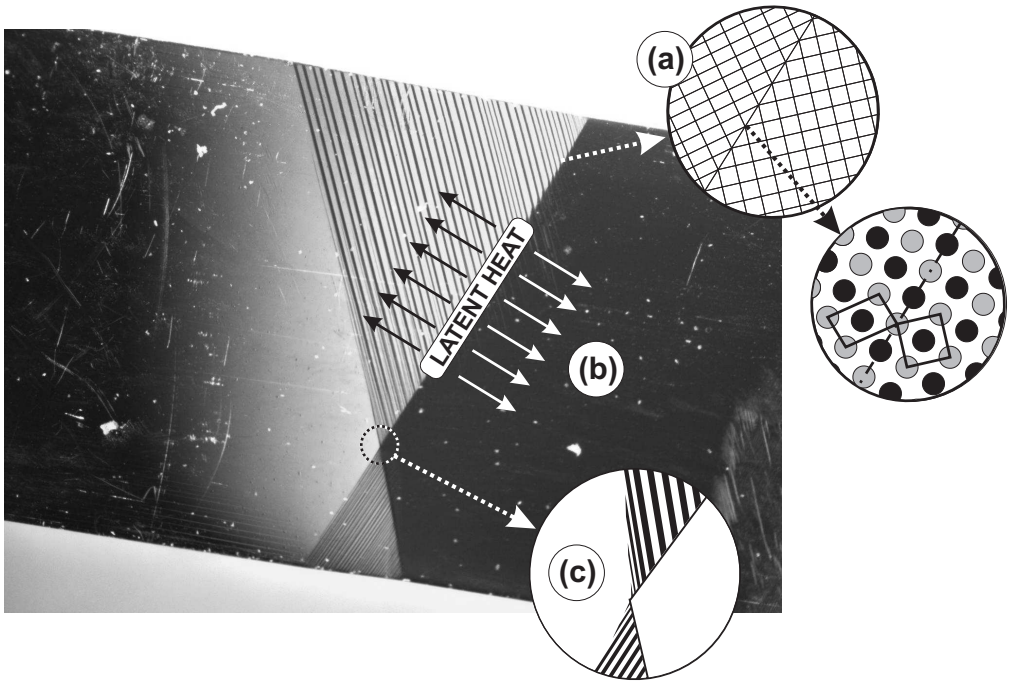

FIGURE 1. Multiscale character of the shape recovery process: The compatibility conditions at the atomistic scale (a) constrains the macroscopic Stefan's problem (b) such that it leads to formation of interfacial microstructures (X–interfaces) at the mesoscale (c).

The given talk illustrated the effect of the mechanical stabilization on the single crystals of the Cu-Al-Ni alloy. Above all, it was shown that this material can be mechanically stabilized by a stress–induced transition into the 2H-martensite, and that this stabilization shifts the transition temperature A_s by several degrees upward (this was documented by acoustic-emission measurements). Results of several experimental observations were presented, from which the most essential were:

(1) The shear softening of the mechanically stabilized martensite was analyzed by ultrasonic methods.
(2) The kinetics of the shape recovery process in a thermal gradient was observed by optical and infrared microscopy. The dependence of the phase front velocity on the magnitude of the gradient was discussed and significant decrease of the temperature around the moving interface was documented.
(3) The kinematic compatibility of the observed interfacial microstructure (the X-interface) was analyzed, whereby a FEM model (see [5] for more details) was used to determine the elastic strain fields enabling the existence of this microstructure.
(4) Using the optical microscopy and the white light interferometry, it was shown that some of the twinned-to-detwinned interfaces occurring during the shape recovery process are not sharp, but have, instead, a smooth character given by a continuous disappearance of thin needles of one martensitic variant in another.
(5) It was shown that the examined material is able to form non-classical interfaces (interfaces between austenite and a crossing–twins microstructure of four martensitic variants).
(6) The fact that the nucleation of austenite preferably occurs in the corners of the specimen was illustrated by a simple experiment.

The lack of today's theoretical understanding of the phenomenon of the mechanical stabilization was highlighted. It can be clearly concluded that the open questions raised within the talk cannot be answered without deeper analysis of the interplay between the geometry (the kinematic compatibility, the anisotropy of elastic properties) and thermodynamics driving the transitions in the SMA single crystals.

References

[1] J.M. Ball and R.D. James, *Fine phase mixtures as minimizers of energy*, Archive for Rational Mechanics and Analysis **100** (1987), 13–52.
[2] K. Bhattacharya, *Microstructure of Martensite.* New York, NY: Oxford Series on Materials Modelling, 2003.
[3] V. Novák et al., *Transformation behavior of prism shaped shape memory alloy single crystals*, Materials Science and Engineering A, **438–440** (2006), 755–762.
[4] H. Seiner et al., *Shape recovery mechanism observed in single crystals of Cu–Al–Ni shape memory alloy*, Phase Transitions, **81** (2008), 537–551.
[5] H. Seiner et al., *Interfacial Microstructures in Martensitic Transitions: From Optical Observations to Mathematical Modeling*, accepted to International Journal for Multiscale Computational Engineering, 2009.

Variational modelling of cavitation and fracture

Duvan Henao Manrique
(joint work with Carlos Mora-Corral)

Motivated by experiments of Petrinic *et al.* [10, 11] on the mechanism of ductile fracture by void growth and coalescence, we consider the problem of formulating a variational model in nonlinear elasticity compatible with both cavitation and the appearance of discontinuities across two-dimensional surfaces. In particular, we consider whether the ideas of the model of cavitation of Müller and Spector [9] can be incorporated into the model of brittle fracture of Francfort and Marigo [4], which treats the propagation of cracks as a De Giorgi free-discontinuity problem.

When the formation of cracks and cavities are taken into account, it is necessary to include the energy due to fracture in the total energy of a deformation. In the classical conception of Griffith [6], the energy due to the breaking of bonds is proportional to the area of the cracks created, as they are seen in the *reference configuration*. In the formulation (due to Francfort and Marigo [4], see [3] and the references therein) using deformations $\mathbf{u} \in SBV(\Omega, \mathbb{R}^3)$, where Ω denotes the reference configuration of the elastic body undergoing the deformation (and $SBV(\Omega, \mathbb{R}^3)$ denotes the set of special functions with bounded variation), this quantity is given by $\mathcal{H}^2(J_{\mathbf{u}})$, where $J_{\mathbf{u}}$ is the set of jump discontinuities of $\mathbf{u}$. This energy, however, is inadequate for cavitation, since in this case fracture is confined to the microscopic scale and becomes visible only in the *deformed configuration*. Supported on the observation by Gent and Wang [5] that a second surface energy, due to the stretching of a fracture surface, must be taken into account, Müller and Spector [9] suggested the addition of a term $\mathcal{E}(\mathbf{u})$ that gives the area of the surface created by $\mathbf{u}$, as it is seen after the deformation takes place. We look, therefore, for minimizers of

$$I(\mathbf{u}) := \int_\Omega W(\mathbf{x}, \nabla \mathbf{u}(\mathbf{x}))\, \mathrm{d}\mathbf{x} + \lambda_1 \mathcal{H}^2(J_{\mathbf{u}}) + \lambda_2 \mathcal{E}(\mathbf{u}), \tag{1}$$

where W denotes the stored-energy function of the body and $\nabla \mathbf{u}$ denotes the approximate gradient of $\mathbf{u}$, among the class of deformations in $SBV(\Omega, \mathbb{R}^3)$ that are one-to-one a.e. and satisfy $\det \nabla \mathbf{u} > 0$ a.e., as well as suitable boundary conditions.

As is costumary in nonlinear elasticity, we assume W to be polyconvex. To obtain the existence of minimizers under this assumption reduces to proving that $\det \nabla \mathbf{u}_j \rightharpoonup \det \nabla \mathbf{u}$ in $L^1(\Omega)$, provided $\{\mathbf{u}_j\}_{j \in \mathbb{N}}$ is a weakly convergent minimizing sequence (in the appropriate topology), and $\mathbf{u}$ is its weak limit. When the coerciveness of W on the deformation gradient is sufficiently strong (if, e.g., $W(\mathbf{x}, \mathbf{F}) \geq C|\mathbf{F}|^p$ with $p > 3$, or $W(\mathbf{x}, \mathbf{F}) \geq C(|\mathbf{F}|^p + |\operatorname{cof} \mathbf{F}|^q)$ with $p \geq 2$ and $q > \frac{p}{p-1}$), the result follows from the classical works by Reshetnyak [12] and Ball [1]. In contrast, when cavitation is allowed (which requires W to have slow growth at infinity), the result is not true in general, as was shown by Ball and Murat [2]. The example of Ball and Murat, however, consists of a sequence in which an arbitrarily large amount of new surface is created. This provided Müller and Spector [9] with a further motivation for the addition of a surface energy, and, by

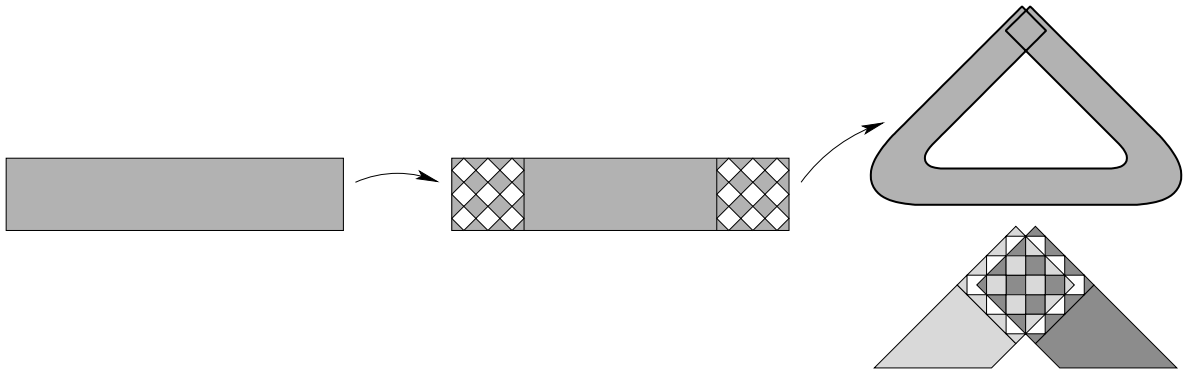

FIGURE 1. Deformation that creates and subsequently interlaces cavities

setting $\mathcal{E}(\mathbf{u}) := \operatorname{Per}\mathbf{u}(\Omega)$, and by introducing a new notion of invertibility, they were indeed able to prove the continuity of the determinant and the existence of minimizers (in the Sobolev case).

The invertibility condition of Müller and Spector [9], called condition INV, plays a major role in their theory. Roughly speaking, it states that cavities produced in one part of the body cannot be filled with material from somewhere else. The need to introduce this condition comes from the fact that in the case of cavitation, apart from being a physical property that one desires to incorporate into the model, the invertibility of deformations is fundamental in order to obtain the mathematical result of existence. In fact, Müller and Spector proved that if $\nabla\mathbf{u}_j \rightharpoonup \nabla\mathbf{u}$ in $L^p(\Omega,\mathbb{R}^{3\times 3})$ (for some $p>1$), the maps $\mathbf{u}_j$ are one-to-one a.e., and $\mathbf{u}$ is one-to-one a.e., *then* $\det\nabla\mathbf{u}_j \rightharpoonup |\det\nabla\mathbf{u}|$ in $L^1(\Omega)$. At the same time, they constructed an example (see Figure 1) of a weakly convergent sequence of deformations (in which cavities are filled with material from somewhere else), for which $\sup_j \operatorname{Per}\mathbf{u}_j(\Omega) < \infty$, which is such that $\mathbf{u}$ is not one-to-one a.e. in spite of the fact that $\mathbf{u}_j$ is one-to-one a.e. for each j. The stronger condition INV, in contrast, is stable with respect to weak convergence in $W^{1,p}(\Omega,\mathbb{R}^3)$, for every $p>2$.

While condition INV offers definite advantages to the analysis of cavitation in the Sobolev setting, it is no longer possible to make use of it when deformations are in SBV. In turns out that the mere formulation of this condition, which is based on the topological degree for Sobolev deformations, requires deformations to be such that their restrictions to almost every surface are continuous. When two-dimensional fracture occurs this continuity property no longer holds. Instead of replacing the condition of invertibility a.e., we propose a model in which the pathological deformations of Figure 1 are allowed to compete in the energy minimization. We observe that this counterexample should have been already ruled out by the addition of a surface energy, for in this sequence (as in the example of Ball and Murat [2]) an arbitrarily large amount of new surface is being created. The difference is that in this example there are pieces of created surface that are in contact with each other. In this situation the contact surface is left surrounded by matter, and does not form part of the boundary of the body. It becomes, therefore, *invisible*, or undetectable to $\operatorname{Per}\mathbf{u}(\Omega)$, the surface energy in [9]. Based

on geometric and analytic considerations, in [8] we redefine $\mathcal{E}(\mathbf{u})$ as follows:

$$\mathcal{E}(\mathbf{u}) := \sup\left\{\int_\Omega [(D_{\mathbf{x}}\mathbf{f})(\mathbf{x},\mathbf{u}(\mathbf{x}))\cdot \operatorname{cof}\nabla\mathbf{u}(\mathbf{x}) + (\operatorname{div}_{\mathbf{y}}\mathbf{f})(\mathbf{x},\mathbf{u}(\mathbf{x}))\det\nabla\mathbf{u}(\mathbf{x})]\,\mathrm{d}\mathbf{x}\right\},$$

where the supremum is taken over all $\mathbf{f}\in C_c^\infty(\Omega\times\mathbb{R}^3,\mathbb{R}^3)$ such that $\|\mathbf{f}\|_\infty\leq 1$. Using this surface energy, which gives correctly the area of the created surface, even when *invisible* surface is created (see [7]), we are able to prove that for sequences with bounded surface energy the condition of invertibility a.e. is stable under the weak limit. Moreover, we obtain new results on the weak continuity of the determinant, and establish the existence of minimizers for (1). Finally, we show that the functional $\mathcal{E}(\mathbf{u})$ is related to a well-known object in the theory of Cartesian currents (namely, the $(n-1)$ vertical part $(\partial G_{\mathbf{u}})_{(n-1)}$ of the current carried by the graph of $\mathbf{u}$), and that the condition $\mathcal{E}(\mathbf{u})<\infty$ is connected to the BV and SBV regularity of the inverses.

References

[1] J. M. Ball, *Convexity conditions and existence theorems in nonlinear elasticity*, Arch. Rational Mech. Anal., 63 (1976/77), pp. 337–403.

[2] J. M. Ball and F. Murat, *$W^{1,p}$-quasiconvexity and variational problems for multiple integrals*, J. Funct. Anal., 58 (1984), pp. 225–253.

[3] B. Bourdin, G. A. Francfort, and J.-J. Marigo, *The variational approach to fracture*, J. Elasticity, 91 (2008), pp. 5–148.

[4] G. A. Francfort and J.-J. Marigo, *Revisiting brittle fracture as an energy minimization problem*, J. Mech. Phys. Solids, 46 (1998), pp. 1319–1342.

[5] A. Gent and C. Wang, *Fracture mechanics and cavitation in rubber-like solids*, J. Mater. Sci., 26 (1991), pp. 3392–3395.

[6] A. A. Griffith, *The phenomena of rupture and flow in solids*, Philos. Trans. Roy. Soc. London Ser. A, 221 (1921), pp. 163–198.

[7] D. Henao and C. Mora-Corral, *Fracture surfaces and the regularity of inverses for BV deformations*. Submitted.

[8] ———, *Invertibility and weak continuity of the determinant for the modelling of cavitation and fracture in nonlinear elasticity*. Preprint OxPDE-09/09 available at http://www.maths.ox.ac.uk/groups/oxpde/technical-report-series.

[9] S. Müller and S. J. Spector, *An existence theory for nonlinear elasticity that allows for cavitation*, Arch. Rational Mech. Anal., 131 (1995), pp. 1–66.

[10] N. Petrinic, J. L. Curiel Sosa, C. R. Siviour, and B. C. F. Elliott, *Improved predictive modelling of strain localisation and ductile fracture in a Ti-6Al-4V alloy subjected to impact loading*, Journal de Physique IV, 134 (2006), pp. 147–155.

[11] N. Petrinic, C. R. Siviour, J. L. Curiel Sosa, and B. C. F. Elliott, *On competing volumetric and deviatoric damage mechanisms in simulation of ductile fracture in Ti64 alloy at high rates of strain*, in Proceedings of Euromech EMMC-10 Conference "Multi-phase and multi-component materials under dynamic loading", Kazimierz Dolny (Poland), 2007, pp. 467–478.

[12] Y. G. Reshetnyak, *Spatial mappings with bounded distortion*, Sibirsk. Mat. Ž., 8 (1967), pp. 629–658.

Characterizing Peridynamics for the Dynamic Motion of Martensitic Interfaces

Kaushik Dayal
(joint work with Kaushik Bhattacharya)

The continuum peridynamic theory of solids was proposed by Silling [1]. The key idea is to replace the local tractions by long-range interactions ("bonds") between every continuum element in the body. This physical picture leads to the balance of momentum in the form

$$\rho\ddot{u}(x,t) = \int_\Omega f(u(x',t) - u(x,t), x, x')\ dx' + b(x,t) \tag{1}$$

In this equation, ρ is the density, u is the displacement field as a function of reference position x and time t, b is the body force density, and the body is denoted by Ω. The function f is the bond force between continuum elements and depends on the referential positions as well as the relative displacement. Hence, f is hueristically analogous to pairwise interactions. Generalizations to multibody interactions have been achieved [2] but we do not consider them here.

Peridynamics is motivated by the fact that the theory does not *a priori* impose any continuity on the displacement field. This makes it an attractive alternative to classical continuum approaches for the modeling of cracks and interfaces and recent efforts have shown some success. We have characterized the motion of martensitic interfaces in peridynamics in one and two dimensions.

In one dimension, we formulate a trilinear material with 2 stable branches and a spinodal, corresponding to a classical nonconvex energy. This is a simple model for phase transformations. As shown in the seminal work of Abeyaratne and Knowles [3, 4], the classical continuum theory with nonconvex energies suffers from a massive loss of uniqueness of dynamic solutions. They propose a method to obtain uniqueness by specifying additional closure equations. These equations contain the physical information that specifies the nucleation and kinetics of phase boundaries.

We examine this question in peridynamics. We begin by explicit time-marching of IBVP problems corresponding to impact and Riemann problems. The results indicate that phase boundaries nucleate without difficulty (unlike many regularized models), and that the motion of phase boundaries resemble traveling waves.

Hence we examine kinetics of phase boundaries directly by searching for traveling waves. We use the ansatz $u(x,t) = u(x - vt)$ and solve numerically the resulting equation:

$$\rho v^2 u(x,t) = \int_\Omega f(u(x',t) - u(x,t), x, x')\ dx' + b(x,t) \tag{2}$$

For a given v, we find $u(x,t)$ and from this extract the thermodynamic driving force that in the classical continuum theory is the conjugate of v [3]. We find that the relation between v and driving force obtained from traveling waves matches

well the similar relation that we obtain from the IBVP problems mentioned above. This suggests that peridynamics has built within it a kinetic relation

We then examine the issue of nucleation. We approach this from the perspective of stability. We find that this naturally leads to the notion of a critical nucleus size, and further that the nucleus size is very strongly dependent on the strain field *outside* the nucleus. For certain examples, we obtain simple scaling laws that are found to match very well with corresponding IBVP calculations.

In two dimensions, we see that peridynamics predicts an unusual mechanism for a twin boundary to pass over an inclusion. The acoustic waves leading the phase boundary nucleate a pair of new twin boundaries on the far side of the inclusion, and these new twin boundaries carry forward the transformation while the original twin boundary comes to rest before the inclusion [5].

References

[1] S. A. Silling, *Reformulation of elasticity theory for discontinuities and long-range forces*, Journal of the Mechanics and Physics of Solids **48** (2000), 175–209.

[2] S. A. Silling, M. Epton, O. Weckner, J. Xu, E. Askari, *Peridynamic States and Constitutive Modeling*, Journal of Elasticity **88** (2007), 151–184.

[3] R. Abeyaratne, J. K. Knowles, *Kinetic relations and the propagation of phase boundaries in solids*, Archive for Rational Mechanics and Analysis **114** (1991), 119–154.

[4] R. Abeyaratne, J. K. Knowles, *On the driving traction acting on a surface of strain discontinuity in a continuum*, Journal of the Mechanics and Physics of Solids **38** (1990), 345–360.

[5] K. Dayal, K. Bhattacharya, *Kinetics of phase transformations in the peridynamic formulation of continuum mechanics*, Journal of the Mechanics and Physics of Solids **54** (2006), 1811–1842.

2D & 3D microstructures studied by TEM & SEM

Dominique Schryvers

The presentation covers several recent examples of atomic and microstructures investigated by transmission electron microscopy (TEM) or scanning electron microscopy (SEM) in different materials and that do or can possibly relate to the multitude of PDE approaches available in this community. The topics presented include (1) shape memory alloys (SMA) with special lattice parameters and microstructures for low hysteresis: $Ti_{50}Ni_{50-y}X_y$ (X=Pd, Au), (2) shape analysis and 3D distribution of Ni_4Ti_3 precipitates by FIB/SEM slice-and-view: comparing stress-free and compressed Ni-Ti material, (3) measuring the full 3D strain field surrounding Ni_4Ti_3 precipitates and fitting it with the R-phase transformation strain, (4) pinning of the martensite structure by dislocations in $Cu_{74.08}Al_{23.13}Be_{2.79}$, explaining unexpected hardening of the martensite.

The first topic investigates the evolution of microstructure by different TEM methods, including conventional imaging, selected area diffraction and some atomic resolution, as the composition of the $Ti_{50}Ni_{50-x}Pd_x$ system is systemically tuned to achieve the compatibility condition between austenite and martensite, i.e. $\lambda_2 = 1$, where λ_2 is the middle eigenvalue of the transformation strain matrix [1]. A sharp drop in hysteresis is observed for SMA satisfying this condition. Changes in

morphology, twinning density and twinning modes are reported along with twinless martensite and exact austenite-martensite interfaces [2]. An in-situ cooling experiment highlights the twinless character of the martensite as well as the jerky growth of the plate. A similar series, although less obvious, can be recognized in the $Ti_{50}Ni_{50-x}Au_x$ system.

In the second contribution the 3D morphology and distribution of lenticular and cylindrical Ni_4Ti_3 precipitates in the austenitic B2 matrix of two different binary Ni-Ti alloys, one stress-free annealed and one aged under compression, have been investigated by a slice-and-view procedure in a Dual-Beam FIB/SEM system. Due to the weak contrast of the precipitates, proper imaging conditions need to be selected first to allow for semi-automated image treatment [3]. From the volume fraction of the precipitates a decrease of the Ni-content can be measured. For the stress-free alloy this resulted in an increase of 125 degrees for the martensitic start temperature. The 3D shape analysis of the stress-free grown precipitates confirms the expected lens-shape, but the precipitates in the compressed material take a more cylindrical shape, probably due to a smaller difference between the lattice mismatch of the precipitate and the matrix. It can further be concluded that the single-variant and aligned precipitates in the compressed material are arranged in pockets of $0.54 \times 1 \times 1\mu m^3$ size defining the space for martensite outbursts. The population of shapes of the stress-free grown precipitates contains more tabular types whereas the compressed sample shows more bladed cases, possibly due to a slight misalignment during compression.

The presence of Ni_4Ti_3 precipitates can introduce an extra transformation step in the B2 to B19′ martensitic transformation in Ni-Ti SMA, related to the so-called R-phase. It is believed that the strain field surrounding the precipitates, caused by the matrix-precipitate lattice mismatch, lies at the origin of this intermediate transformation step, although the effect of local concentration gradients should not be forgotten [4]. Atomic-resolution TEM in combination with geometrical phase analysis (GPA) is used to measure the elastic strain field surrounding these precipitates. By combining measurements from two different crystallographic directions, the three-dimensional strain matrix is determined from two-dimensional measurements. Comparison of the measured strain matrix to the eigenstrain of the R-phase shows that both are very similar and that the introduction of the R-phase might indeed compensate the elastic strain introduced by the precipitate [5].

A single crystal of $Cu_{74.08}Al_{23.13}Be_{2.79}$ undergoes a martensitic phase transition at 246K and 232K under heating and cooling, respectively. The phase fronts between the austenite and martensite regions of the sample are weakly mobile with a power law resonance under external stress fields. Surprisingly, the martensite phase is elastically much harder than the austenite phase showing that interfaces between various crystallographic variants are strongly pinned and cannot be moved by external stress while the phase boundary between the austenite and martensite regions in the sample remains mobile. Transmission Electron Microscopy shows

that the pinning is generated by dislocations, which are inherited from the austenite phase. These dislocations hinder the movement of partial dislocations that are active in generating the proper stacking sequence of the stable 18R martensite structure, as could be deduced from still images as well as in situ cooling experiments. The same type of dislocations are also found attached to the martensite twin boundaries [6].

References

[1] Zhiyong Zhang, Richard D. James and Stefan Müller, *Energy barriers and hysteresis in martensitic phase transformations*, Acta Materialia **57** (2009), 4332–4352.

[2] Rémi Delville, Dominique Schryvers, Zhiyong Zhang and Richard D. James, *Transmission electron microscopy investigation of microstructures in low-hysteresis alloys with special lattice parameters*, Scripta Materialia **60** (2009), 293–296.

[3] Shansan Cao, Wim Tirry, Wouter Van den Broek and Dominique Schryvers, *Optimization of a FIB/SEM slice-and-view study of the 3D distribution of Ni_4Ti_3 precipitates in Ni-Ti*, Journal of Microscopy **233** (2009), 61–68.

[4] Zhiqing Yang, Wim Tirry and Dominique Schryvers, *Analytical TEM investigations on concentration gradients surrounding Ni_4Ti_3 precipitates in Ni-Ti shape memory material*, Scripta Materialia **52** (2005), 1129–1134.

[5] Wim Tirry and Dominique Schryvers, *Linking a completely three-dimensional nanostrain to a structural transformation eigenstrain*, Nature Materials **8, No 9** (2009), 752–757.

[6] E.K.H. Salje, H. Zhang, H. Idrissi, D. Schryvers, M.A. Carpenter, X. Moya and A. Planes, *Mechanical Resonance of the Austenite/Martensite Interface and the Pinning of the Martensitic microstructures by dislocations in $Cu_{74.08}Al_{23.13}Be_{2.79}$*, Phys. Rev. B (accepted for publication).

Self-Organized Magneto-Electrics

Manfred Wuttig

The presentation given on September 15 at the Oberwolfach workshop on PDE's in materials sciences dealt with magnetoelectrics, i.e. materials which are simultaneously ferromagnetic and ferroelectric. The presentation concentrated on ways to synthesize composite magnetoelectrics that are characterized by the high Curie temperatures of the components. Three different types of syntheses were presented and the properties of the resulting magnetoelectric composites discussed: spinodal and pseudo-spinodal decomposition as well as diblock copolymer ordering. The concepts of the three are shown in Fig. 1 together with the nanostructures which can be obtained.

Details on the synthesis and properties of these structures follow.

The NFO/PZT composites was produced by crystallizing and spinodally decomposing a gel in a magnetic field below the Curie temperature of NFO. The gel had been formed by spinning a sol onto a silicon substrate. The ensuing microstructure, characterized by atomic force microscopy, magnetic force microscopy, Lorentz transmission electron microscopy, and scanning electron microscopy, is nanoscopically periodic and, determined by the direction of magnetic annealing field, anisotropic as can be seen in Fig. 1, bottom left. The wavelength of the PZT/NFO alternation, 25 nm, agrees within a factor of 2 with the theoretically

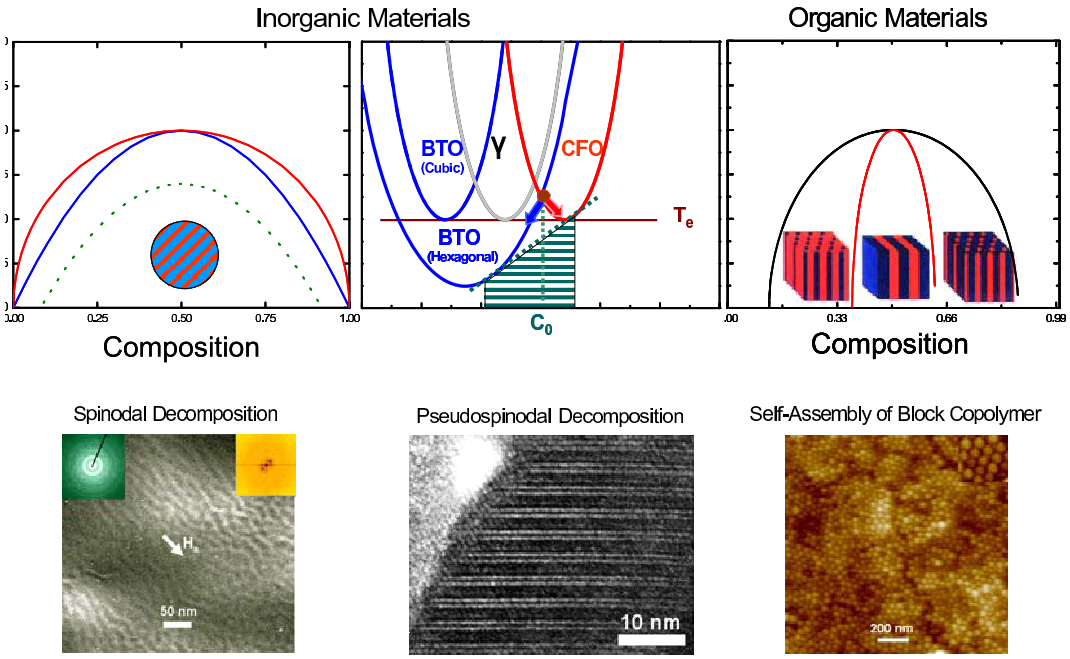

FIGURE 1. Principles of Self-Organization of Magnetoelectric Nanocomposites
Left, top; spinodal decomposition, the composition dependence of the solute solubility and spinodal are shown in red and blue, respectively, decomposition below the spinodal results in the encirceled blue/red periodic structure; such a structure was synthesized by decomposing a nickel-ferrite (NFO)/lead-zirconium-titanate (PZT) gel in a magnetic field.
Left, bottom; magnetoelectric NFO/PZT nanostructure as viewed by AFM.
Center, top; pseudo-spinodal decomposition, the free energies of CFO (red) and the hexagonal as well as cubic phases of barium titanate (BTO, blue) are shown as a function of composition; If the average composition C_0 is located at the red/blue intersection continuous spinodal-like decomposition can occur.
Center, bottom; Pseudo-spinodal decomposition of CFO/BTO.
Right, top; typical phase diagram of a diblock copolymer.
Right, bottom; AFM image of hexagonally short range ordered (note the Fourier transform in the inset) magnetoelectric nanostructure of a decomposed amphiphilic 65/35 polystyrene- block-polyethylene oxide doped with CFO and PZT, respectively.

estimated value. The macroscopic ferromagnetic and magnetoelectric responses correspond qualitatively and semiquantitatively to the features of the nanostructure. As shown in the inset of Fig. 2, the maximum of the field dependent magnetoelectric susceptibility equals 1.8 V/cm Oe [1].

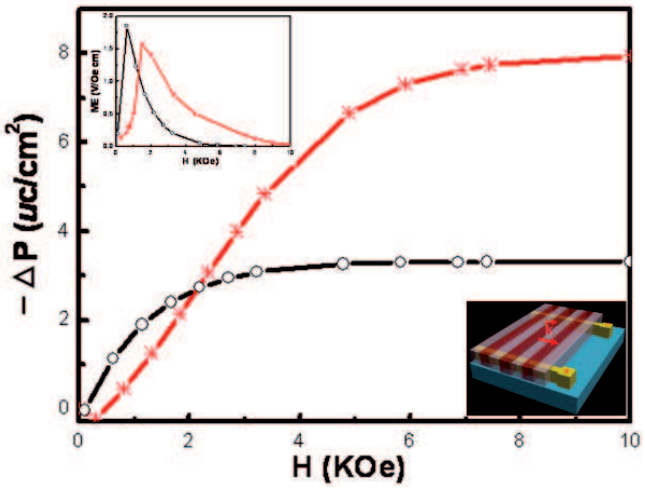

FIGURE 2. ME characteristic and ME susceptibilities (upper inset) of a PZT/NFO film composite annealed for 12 hours at 4800C in an in- and out-of- plane, red and black line, respectively. The inset on the lower right indicates the placement of the electrodes used to apply the electric field.

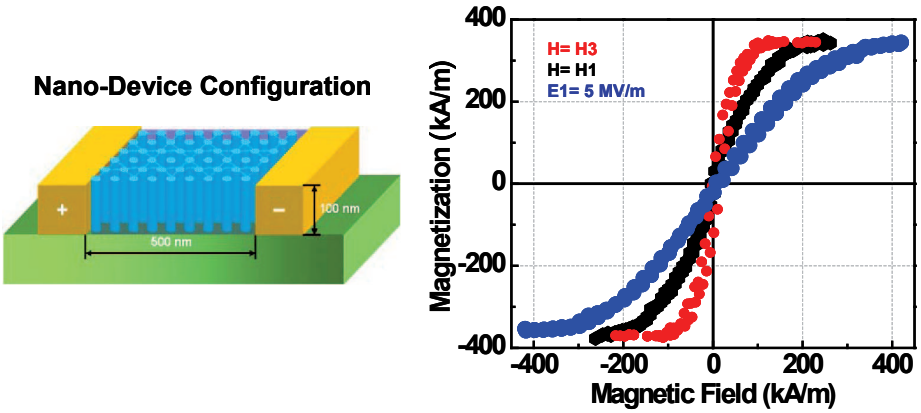

FIGURE 3. left, schematic of an electroded $[PS(PZT)]_{65}$-block-$[PEO(CFO)]_{35}$ sample. The electric field E_1 was applied at the electrodes marked "+" and "−". Right, ferromagnetic and ME characteristics of the hexagonal CFO cylinder array embedded in the PZT matrix magnetized parallel and perpendicularly to their axes, H_3, red, and H_1, black, and, with an applied magnetic, H_3 plus electric field, E_1, blue. The permeability of the nanostructure can be changed by the application of an electric field. The ratio of the initial permeabilities, $\mu(H_3)/\mu(H_3 + E_1) \approx 500\%$.

The magnetoelectric (ME) composite shown at the center of Fig. 1 was synthesized using coassembly of two inorganic precursors with a block copolymer. This solution processed material consists of hexagonally arranged ferromagnetic

cobalt ferrite ($CoFe_2O_4$, CFO) nano cylinders within a matrix of ferroelectric lead zirconium titanate ($Pb_{1.1}Zr_{0.53}Ti_{0.47}O_3$, PZT) when thin films were prepared by spin coating. The initial magnetic permeability of the self-assembled CFO/PZT nanocomposite changes by a factor of 5 by the application of 2.5 V, see Fig. 3. Hence, a block copolymer can be used to simultaneously template two inorganic phases to form a nanoscale composite [2].
The spinel-perovskite $BaTiO_3$-$CoFe_2O_4$ nanolamellar bicrystal shown at the bottom center of Fig. 1 was also fabricated using sol/gel techniques. $(1-10)$ interfaces join the $BaTiO_3$ and $CoFe_2O_4$ single crystalline periodically arranged lamellae that have a common [111] direction. The superlattice of approximately 2 nm wavelength is magnetoelectric with a frequency dependent coupling coefficient of 20mV/Oe cm at 100Hz, see Fig. 4, which is the largest currently known in a crystal at room temperature. The $BaTiO_3$ component is a ferroelectric relaxor with a Vogel-Fulcher temperature of 311 K. The relaxor behavior gives rise to a magnetic tunability of the relative dielectric constant $< \epsilon_r >^{-1} d\epsilon_r/dH \approx 10^{-2}$. Since the material can be produced by standard ceramic processing methods, the discovery represents great potential for magnetoelectric devices [3].
Electric and magnetic fields have drastic effects on the formation of amphiphylically doped magnetoelectric diblock copolymer nanostructures. Perfectly long range ordered lamellar structures are formed when $[PS(PZT)]_{50}$-block-$[PEO(CFO)]_{50}$ is formed in an electric field while onion-like structures are formed when a magnetic field is applied. The electrically induced order is facilitated by the large difference in the dielectric constants of the magnetically and electrically doped blocks. A Lorentz force is likely responsible for the magnetically induced onion structure [4].

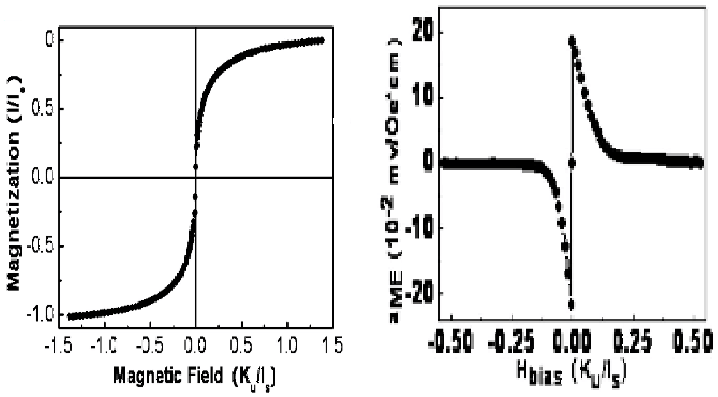

FIGURE 4. Magnetic properties of a $[BaTiO_3]_{50} - [CoFe_2O_4]_{50}$ Bi-Crystal.
Left, room temperature magnetic hysteresis loop;
Right, magnetoelectric coupling constant, α_{ME}, determined with a magnetic AC field of 100Hz as a function of the normalized magnetic bias field, the maximum occurs at a bias field of 10 Oe.

References

[1] S. Ren and M. Wuttig, *Spinodal Synthesis of a PZT/NFO magnetoelectric*, Appl. Phys. Letters **91**, 083501 (2007)

[2] S. Ren, R.M. Briber and M. Wuttig, *Diblock Copolymer Based Self-Assembled Nano-Magneto-Electric*, Applied Physics Letters **93**, 173507 (2008)

[3] Shenqiang Ren, Mark Laver and Manfred Wuttig, *Nanolamellar Magnetoelectric* $BaTiO_3 - CoFe_2O_4$ *Bi-Crystal*, to appear in Applied Physics Letters

[4] S. Ren, R.M. Briber and M. Wuttig, APS Spring Meeting 2009

How many conditions are there on a phase boundary

Yury Grabovsky and Lev Truskinovsky

1. General theory

Consider strong local minimizers of

$$E(\boldsymbol{y}) = \int_\Omega W(\nabla \boldsymbol{y}) d\boldsymbol{x} - \int_{\partial\Omega} (\boldsymbol{t}, \boldsymbol{y}) dS(\boldsymbol{x}).$$

where $W : \mathbb{R}^{m\times d} \to \mathbb{R}$ is smooth and highly non-convex energy density. The specific boundary conditions will be of no importance for the purposes of this talk. In the absence of quasiconvexity the existence of global minimizers is not assured and it is possible that no strong local minimizers exist as well. However, the mechanics literature is full of examples of equilibrium configurations featuring smooth surfaces of strain discontinuity Σ (e.g. [2, 3, 4, 5, 10, 12, 13] and the references therein). In other words for every $\boldsymbol{x}_0 \in \Sigma$

$$\lim_{\epsilon\to 0} \boldsymbol{F}(\boldsymbol{x}_0 + \epsilon \boldsymbol{z}) = \overline{\boldsymbol{F}}(\boldsymbol{z}) = \begin{cases} \boldsymbol{F}_+, & \text{if } \boldsymbol{z}\cdot\boldsymbol{n} > 0, \\ \boldsymbol{F}_-, & \text{if } \boldsymbol{z}\cdot\boldsymbol{n} < 0. \end{cases} \tag{1}$$

Classical jump conditions that consist of kinematic compatibility

$$[\![\boldsymbol{F}]\!] = \boldsymbol{a}\otimes\boldsymbol{n}, \tag{2}$$

where $[\![\boldsymbol{F}]\!] = \boldsymbol{F}_+ - \boldsymbol{F}_-$, continuity of tractions

$$[\![\boldsymbol{P}]\!]\boldsymbol{n} = \boldsymbol{0}, \tag{3}$$

where $\boldsymbol{P} = W_{\boldsymbol{F}}$ is the Piola-Kirchhoff stress tensor, and the Maxwell relation [1, 9]

$$[\![W]\!] - (\{\!\{\boldsymbol{P}\}\!\}, [\![\boldsymbol{F}]\!]) = 0, \tag{4}$$

where $\{\!\{\boldsymbol{P}\}\!\} = (\boldsymbol{P}_+ + \boldsymbol{P}_-)/2$ are well-known restrictions on the values $\boldsymbol{F}_\pm$ defined in (1). But is this the complete list? Let us examine the jump conditions from the geometric point of view.

Definition 1. *The set of matrices* $\boldsymbol{F}_- \in \mathbb{R}^{m\times d}$ *such that there exists a counterpart* $\boldsymbol{F}_+$ *satisfying the classical jump conditions is called the* Maxwell set $\mathfrak{M}$.

There are $2md + m + d - 1$ unknowns $\boldsymbol{F}_+$, $\boldsymbol{F}_-$, $\boldsymbol{a}$, $\boldsymbol{n}$ in $md + m + 1$ equations (2)–(4). Hence, if one fixes $\boldsymbol{F}_- \in \mathfrak{M}$ there will be a $d-2$-parametric family of $\boldsymbol{F}_+$ satisfying all jump conditions. In other words, For $\boldsymbol{F}_- \in \mathfrak{M}$ we can construct a $d-2$-parametric family of configurations of the type

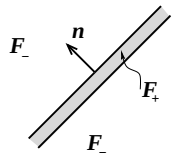

Observations suggest that such solutions exist only for special values of $\boldsymbol{F}_-$ and when they do exist they do not appear as a continuous family. Therefore, some jump conditions appear to be missing. The new condition is very simple

$$[\![\boldsymbol{P}]\!]^T [\![\boldsymbol{F}]\!] \boldsymbol{n} = \boldsymbol{0}. \tag{5}$$

It appeared before in special cases in the works of Gurtin [7] Silling [15] and Šilhavý [14].

If the continuity of tractions (3) expresses equilibrium with respect to perturbations of deformation, keeping the surface of discontinuity immobile in Lagrangian coordinates, the Maxwell condition expresses equilibrium with respect to smooth perturbations of the shape of the surface Σ, the new condition expresses equilibrium with respect to the roughening of Σ schematically depicted in the figure below

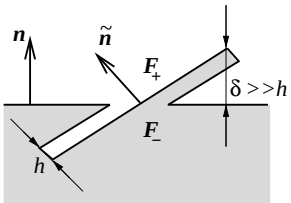

We refer to [6] for the formal proof. Condition (5) leads to the notion of the *jump set*.

Definition 2. *The set of matrices $\boldsymbol{F}_- \in \mathfrak{M}$ such that there exists a counterpart $\boldsymbol{F}_+$ satisfying the classical jump conditions and $[\![\boldsymbol{P}]\!]^T \boldsymbol{a} = \boldsymbol{0}$ is called the jump set* $\mathfrak{J}$

The jump set and the Maxwell set are related geometrically.

THEOREM **1.** *If the acoustic tensor is non-singular then $\partial\mathfrak{M} \subset \mathfrak{J}$.*

Proof. Suppose $(\boldsymbol{F}_0, \boldsymbol{a}_0, \boldsymbol{n}_0)$ is a solution. Solve $W_{\boldsymbol{F}}(\boldsymbol{F} + \boldsymbol{a} \otimes \boldsymbol{n})\boldsymbol{n} - W_{\boldsymbol{F}}(\boldsymbol{F})\boldsymbol{n} = \boldsymbol{0}$ for $\boldsymbol{a}$ near $(\boldsymbol{F}_0, \boldsymbol{a}_0, \boldsymbol{n}_0)$

$$p^*(\boldsymbol{F}, \boldsymbol{n}) = W(\boldsymbol{F} + \boldsymbol{a} \otimes \boldsymbol{n}) - W(\boldsymbol{F}) - (W_{\boldsymbol{F}}(\boldsymbol{F})\boldsymbol{a}, \boldsymbol{n})$$

$p^*(\boldsymbol{F}, \boldsymbol{n}) = 0$ has a solution $\boldsymbol{n}$ for all $\boldsymbol{F} \approx \boldsymbol{F}_0$ if there is $\dot{\boldsymbol{n}} \perp \boldsymbol{n}$ s.t. $\dot{p^*} = 0$.

$$\dot{p}^* = ([\![\boldsymbol{P}]\!]^T \boldsymbol{a}_0, \dot{\boldsymbol{n}}) + ([\![\boldsymbol{P}]\!] \boldsymbol{n}_0, \dot{\boldsymbol{a}}) = ([\![\boldsymbol{P}]\!]^T \boldsymbol{a}_0, \dot{\boldsymbol{n}}).$$

□

Now we can answer the question in the title of the paper. As before we have $2md + m + d - 1$ unknowns $\boldsymbol{F}_+$, $\boldsymbol{F}_-$, $\boldsymbol{a}$, $\boldsymbol{n}$ and $md + m + d$ equations (2)–(5). Indeed, the vanishing of the dot product of the left-hand side of (5) with $\boldsymbol{n}$ is the well-known Hill orthogonality relation [8]. Hence out of the d equations (5) no more than $d-1$ can be independent. The examples in the next section show that the jump set is indeed $md-1$-dimensional, indicating that the $d-1$ equations in (5) are indeed independent. We conclude that the set of admissible pairs $\boldsymbol{F}_\pm$ at the interface is a $md-1$-parametric family parameterized by $\boldsymbol{F}_- \in \mathfrak{J}$.

2. Examples

Our first example is antiplane shear. This example was studied by Silling [15], who computed the jump set and used to show non-existence of classical solutions to certain boundary value problems. Consider the energy density

$$W : \mathbb{R}^2 \to \mathbb{R}, \qquad W(\boldsymbol{F}) = \min\{\frac{1}{2}\mu_+|\boldsymbol{F}|^2 + w_+, \frac{1}{2}\mu_-|\boldsymbol{F}|^2 + w_-\},$$

where $\mu_+ > \mu_- > 0$ — shear moduli of the phases, $w_+ < w_-$. The Maxwell set and the jump set are shown in the figure below.

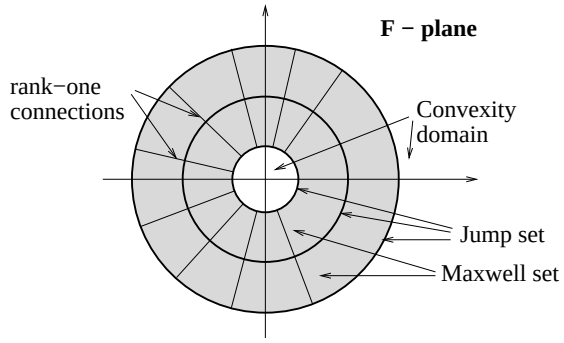

The second example is plane elasticity with the energy density given by

$$\widehat{W}(\boldsymbol{\varepsilon}) = \min\{\frac{1}{2}(\mathsf{C}_+(\boldsymbol{\varepsilon} - \boldsymbol{\varepsilon}_+^\circ), \boldsymbol{\varepsilon} - \boldsymbol{\varepsilon}_+^\circ) + \widehat{w}_+, \frac{1}{2}(\mathsf{C}_-(\boldsymbol{\varepsilon} - \boldsymbol{\varepsilon}_-^\circ), \boldsymbol{\varepsilon} - \boldsymbol{\varepsilon}_-^\circ) + \widehat{w}_-\}$$

If $[\![\mathsf{C}]\!]$ is invertible, the energy density can be simplified to

$$W(\boldsymbol{\varepsilon}) = \min\{\frac{1}{2}(\mathsf{C}_+\boldsymbol{\varepsilon}, \boldsymbol{\varepsilon}) + \widehat{w}_+, \frac{1}{2}(\mathsf{C}_-\boldsymbol{\varepsilon}, \boldsymbol{\varepsilon}) + \widehat{w}_-\}$$

via a simple affine transformation (see for instance [11])

$$\widehat{W}(\boldsymbol{\varepsilon}) = W(\boldsymbol{\varepsilon} - \overline{\boldsymbol{\varepsilon}}) + (\boldsymbol{\sigma}^\circ, \boldsymbol{\varepsilon}) - \frac{1}{2}(\boldsymbol{\sigma}^\circ, \overline{\boldsymbol{\varepsilon}}),$$

where

$$\overline{\boldsymbol{\varepsilon}} = [\![\mathsf{C}]\!]^{-1}[\![\mathsf{C}\boldsymbol{\varepsilon}^\circ]\!], \qquad \boldsymbol{\sigma}^\circ = \{\!\{\mathsf{C}\}\!\}\overline{\boldsymbol{\varepsilon}} - \{\!\{\mathsf{C}\boldsymbol{\varepsilon}^\circ\}\!\} = \mathsf{C}_\pm(\overline{\boldsymbol{\varepsilon}} - \boldsymbol{\varepsilon}_\pm^\circ),$$

$$w_\pm = \widehat{w}_\pm - \frac{1}{2}(\boldsymbol{\sigma}^\circ, \boldsymbol{\varepsilon}_\pm^\circ).$$

Assuming that $\mathsf{C}_+ > \mathsf{C}_-$ and isotropic we obtain the following picture of the jump set and the Maxwell set

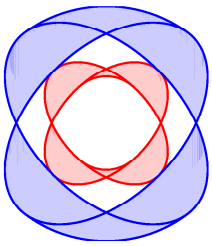

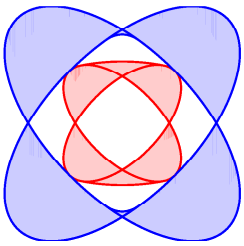

The left figure corresponds to the positive definite case and the left figure to the elliptic, non positive definite case. The picture is drawn in the (X, Y)-plane, where

$$X = \frac{\varepsilon_1 + \varepsilon_2}{\sqrt{2}}, \qquad Y = \frac{\varepsilon_2 - \varepsilon_1}{\sqrt{2}},$$

since the membership in $\mathfrak{M}$ and $\mathfrak{J}$ depend only on the eigenvalues ε_1 and ε_2 of $\boldsymbol{\varepsilon} = (\boldsymbol{F} + \boldsymbol{F}^T)/2$. The blue color corresponds to $\boldsymbol{\varepsilon}_-$ and the red to $\boldsymbol{\varepsilon}_+$, where it is assumed that $\mathsf{C}_+ > \mathsf{C}_-$. If in the case of the antiplane shear the jump set was exactly the boundary of the Maxwell set, then in the case of plane strain elasticity the inclusion $\partial\mathfrak{M} \subset \mathfrak{J}$ is strict.

References

[1] J. D. Eshelby. Energy relations and energy momentum tensor in continuum mechanics. In M. Kanninen, W. Adler, A. Rosenfeld, and R. Jaffee, editors, *Inelastic behavior of solids*, pages 77–114. McGraw-Hill, New York, 1970.

[2] R. L. Fosdick and G. MacSithigh. Helical shear of an elastic, circular tube with a nonconvex stored energy. *Arch. Rational Mech. Anal.*, 84(1):31–53, 1983.

[3] A. Freidin, Y. Fu, L. L. Sharipova, and E. N. Vilchevskaya. Spherically symmetric two-phase deformations and phase transition zones. *Int. J. Solids Struct.*, 43:4484–4508, 2006.

[4] A. B. Freidin. On new phase inclusions in elastic solids. *ZAMM Z. Angew. Math. Mech.*, 87(2):102–116, 2007.

[5] E. Fried. Construction of two-phase equilibria in a nonelliptic hyperelastic material. *J. Elasticity*, 31(2):71–123, 1993.

[6] Y. Grabovsky and L. Truskinovsky. A new condition of phase equilibrium in nonlinear elasticity. Submitted.

[7] M. E. Gurtin. Two-phase deformations of elastic solids. *Arch. Ration. Mech. Anal.*, 84(1):1–29, 1983.

[8] R. Hill. Energy momentum tensors in elastostatics:some reflections on the general theory. *J. Mech. Phys. Solids*, 34:305–317, 1986.

[9] R. D. James. Finite deformation by mechanical twinning. *Arch. Ration. Mech. Anal.*, 77(2):143–176, 1981.

[10] J. K. Knowles and E. Sternberg. On the failure of ellipticity and the emergence of discontinuous deformation gradients in plane finite elastostatics. *J. Elasticity*, 8(4):329–379, 1978.

[11] T. Mura. *Micromechanics of defects in solids*. Springer, 1987.

[12] P. Rosakis. Compact zones of shear transformation in an anisotropic solid. *J. Mech. Phys. Solids*, 40(6):1163–1195, 1992.

[13] M. Šilhavý. *The mechanics and thermodynamics of continuous media*. Texts and Monographs in Physics. Springer-Verlag, Berlin, 1997.

[14] M. Šilhavý. Maxwell's relation for isotropic bodies. In *Mechanics of material forces*, volume 11 of *Adv. Mech. Math.*, pages 281–288. Springer, New York, 2005.

[15] S. A. Silling. Consequences of the Maxwell relation for anti-plane shear deformations of an elastic solid. *J. Elasticity*, 19(3):241–284, 1988.

Sub-linear scaling methods for electronic structure computations in materials

Carlos J. García-Cervera
(joint work with Jianfeng Lu, Weinan E)

We discuss the class of sub-linear scaling algorithms for analyzing the electronic structure of crystalline solids with isolated defects introduced in [1], in the context of Kohn-Sham Density-Functional Theory (DFT) [2].

1. Kohn-Sham DFT

The rescaled energy functional for the Kohn-Sham density functional theory model is [2]

$$I_\varepsilon(\{\psi_k\}) = \frac{\varepsilon^2}{2}\sum_k \int_{\mathbb{R}^3} |\nabla\psi_k(y)|^2\,\mathrm{d}y + \int_{\mathbb{R}^3} \epsilon_{\mathrm{xc}}(\varepsilon^3\rho)\rho(y)\,\mathrm{d}y + \frac{\varepsilon}{2}\iint_{\mathbb{R}^3\times\mathbb{R}^3} \frac{(\rho-m)(y)(\rho-m)(y')}{|y-y'|}\,\mathrm{d}y\,\mathrm{d}y', \tag{1}$$

where the wave functions $\{\psi_j\}$ are orthogonal. The electron density is defined as $\rho(\boldsymbol{x}) = 2\sum_j |\psi_j(\boldsymbol{x})|^2$, and ε is a dimensionless interatomic lengthscale. In (1) we have adopted the local density approximation for the exchange and correlation energy [2]. The ionic function m defines the molecular environment. For simplicity of presentation the nonlocal pseudopotential is not included here. Similar results can be obtained when it is included.

The associated Euler-Lagrange equations are

$$-\frac{\varepsilon^2}{2}\Delta\psi_k + V_{\mathrm{xc}}(\varepsilon^3\rho)\psi_k - \phi\psi_k + \sum_{k'}\lambda_{kk'}\psi_{k'} = 0; \quad -\Delta\phi = 4\pi\varepsilon(m-\rho). \tag{2}$$

Here the λ's are the Lagrange multipliers for the orthonormality constraints, ϕ is the Coulombic potential generated by the charge distribution of electrons and ions, and $V_{\mathrm{xc}}(\varepsilon^3\rho) = \epsilon_{\mathrm{xc}}(\varepsilon^3\rho) + \epsilon'_{\mathrm{xc}}(\varepsilon^3\rho)\varepsilon^3\rho$.

The wave functions $\{\psi_k\}$ are far from being unique. We will assume that the collection of $\{\psi_k\}$ can be chosen as $\{\psi_\alpha(y_i,(x-x_i)/\varepsilon)\}$, where α, which ranges from 1 to $n_0/2$, is the index for the occupied states. $\psi_\alpha(y,\cdot)$ is localized at 0, *i.e.*, it decays away from the origin. Thus $\psi_\alpha(y_i,(x-x_i)/\varepsilon)$ is localized at the atomic position x_i. If the system is in equilibrium or under homogeneous deformation, $\{\psi_\alpha(y_i,(x-x_i)/\varepsilon)\}$ can be chosen as the well-known Wannier function [3] of the α-th energy band centered at x_i.

We take the following ansatz:

$$\psi_\alpha(y,z) = \frac{1}{\varepsilon^{3/2}}\psi_{\alpha,0}(y,z) + \frac{1}{\varepsilon^{1/2}}\psi_{\alpha,1}(y,z) + \varepsilon^{1/2}\psi_{\alpha,2}(y,z) + \cdots. \tag{3}$$

As discussed above, $\psi_\alpha(y,z)$ decays when z becomes large, $\rho(y,z)$ and $\phi(y,z)$ are periodic in z. In the limit as $\varepsilon\to 0$, by the decay property, we obtain, at leading

order $\rho_0(y,z) = 2\sum_\alpha \sum_{z_j\in L}|\psi_{\alpha,0}(y,z-z_j)|^2$. Similarly, for the orthonormality constraint, we have

$$\int_{\mathbb{R}^3} \psi^*_{\alpha,0}(y,z-z_i)\psi_{\alpha',0}(y,z-z_j)\,\mathrm{d}z = \delta_{\alpha\alpha'}\delta_{ij}/\det((\boldsymbol{I}+\nabla u)(x)), \tag{4}$$

with $(\boldsymbol{I}+\nabla u)(x)$ the local deformation gradient. Taking these into consideration and expanding the Euler-Lagrange equations, we get the leading order equations:

$$\begin{aligned} &-\frac{1}{2}\Delta_2^x\psi_{\alpha,0}(y,z) + V_{\mathrm{xc}}(\rho_0)\psi_{\alpha,0}(y,z) - \phi_0(y,z)\psi_{\alpha,0}(y,z) \\ &\qquad + \sum_{\alpha',z_j\in L}\lambda_{\alpha\alpha',z_j0}\psi_{\alpha',0}(y,z-z_j) = 0; \end{aligned} \tag{5}$$

$$-\Delta_2^x\phi_0(y,z) = 4\pi(m_0-\rho_0)(y,z). \tag{6}$$

Here the λ's are Lagrange multipliers. Higher order equations can also be obtained [1]. Notice that the problem becomes effectively local, which means that the local electronic structure at different macro-scale locations are essentially independent of each other and can be solved independently [4, 1].

2. Sublinear scaling algorithm

We divide the localized orbitals of the electrons into two sets: One set associated with the atoms in the region where the deformation of the material is smooth (smooth region), and other set associated with the atoms around the defects (non-smooth region). The orbitals associated with atoms in the smooth region can be approximated accurately using asymptotic analysis. The results can then be used in the original formulation to find the orbitals in the non-smooth region.

Let K, K_s and K_{ns} denote the collection of indices for the wave functions associated with the whole domain, atoms in the smooth region and atoms in the non-smooth region respectively. Note that $K = K_s \cup K_{ns}$, and $K_s \cap K_{ns} = \emptyset$. As before, the electronic structure in the non-smooth region is solved by minimizing the original energy functional, but with the orbitals associated with the atoms in the smooth region already given:

$$\begin{aligned} \inf_{\{\psi_k\}_{k\in K_{ns}}} \frac{1}{2}\sum_{k\in K}\sum_{j\in K}\Big(&\int_{\mathbb{R}^3}(\nabla\psi_k)^{\mathrm{T}}(\boldsymbol{S}^{-1})_{kj}\nabla\psi_j\,\mathrm{d}y \\ &+ \int_{\mathbb{R}^3}\epsilon_{\mathrm{xc}}(\rho)\rho(y)\,\mathrm{d}y + \frac{1}{2}\iint_{\mathbb{R}^3\times\mathbb{R}^3}\frac{(\rho-m)(y)(\rho-m)(y')}{|y-y'|}\,\mathrm{d}y\,\mathrm{d}y' \end{aligned} \tag{7}$$

Here, we have adopted the non-orthogonal formulation [5, 6], so that ρ is defined as

$$\rho(y) = 2\sum_{ij}\psi_i(y)(\boldsymbol{S}^{-1})_{ij}\psi_j(y). \tag{8}$$

The problem is to determine the electronic structure for the non-smooth region given the environment of the smooth region, i.e. given $\{\psi_k\}_{k\in K_s}$, we need to find $\{\psi_k\}_{k\in K_{ns}}$.

We define an environment region, with indices $K_{env} \subset K_s$. This environment region contains the indices of the wave functions that overlap with the non-smooth region. Due to the localization of the orbitals, we can approximate the density by

$$\rho_{ns}(y) = 2 \sum_{i,j \in K_{ns} \cup K_{env}} \psi_i (\widetilde{S}^{-1})_{ij} \psi_j(y), \quad y \in \Omega_{ns}, \tag{9}$$

where we have truncated the overlap matrix, and only consider the wave functions in the non-smooth region, and the environment region:

$$\widetilde{S}_{ij} = \int_{\mathbb{R}^3} \psi_i(y)\psi_j(y)\, dy, \quad i,j \in K_{ns} \cup K_{env}. \tag{10}$$

Let $y(\Omega'_{ns})$ be a domain that contains the support of the orbitals associated with atoms in the non-smooth region. The functional in (7) can now be simplified to:

$$\begin{aligned} \inf_{\{\psi_k\}_{k\in K_{ns}}} & \frac{1}{2} \sum_{k\in K} \sum_{j\in K} \Big(\int_{\mathbb{R}^3} (\nabla \psi_k)^{\mathrm{T}} (\boldsymbol{S}^{-1})_{kj} \nabla \psi_j \,\mathrm{d}y + \int_{\mathbb{R}^3} (V_{ps}\psi_k)(\boldsymbol{S}^{-1})_{kj}\psi_j \,\mathrm{d}y \Big) \\ & + \int_{y(\Omega'_{ns})} \epsilon_{\mathrm{xc}}(\rho)\rho(y)\,\mathrm{d}y + \frac{1}{2} \iint_{y(\Omega'_{ns})\times\mathbb{R}^3} \frac{(\rho-m)(y)(\rho-m)(y')}{|y-y'|}\,\mathrm{d}y\,\mathrm{d}y' \end{aligned} \tag{11}$$

There are several interaction terms that have to be considered. The first is the the Coulomb term. This situation is identical to the TFW case, and we treat the long range interactions (like the nonlocal pseudopotential) in the same way. Other than these long range interactions, the overlap between the wave functions in the smooth region and the wave functions in the non-smooth region also needs to be taken into consideration. It may seem at a first sight that to evaluate (11), for terms like

$$\int_{\mathbb{R}^3} (\nabla \psi_k)^{\mathrm{T}} (\boldsymbol{S}^{-1})_{kj} \nabla \psi_j \,\mathrm{d}y,$$

all the wave functions should be included, which will make the calculation impossible. Fortunately, since we are working with localized wave functions, only a small number of wave functions in the smooth region need to be taken into account.

References

[1] C.J. García-Cervera, J. Lu, and W. E. Asymptotics-based sublinear scaling algorithms and application to the study of the electronic structure of materials. *Comm. Math. Sci.*, 5(4):999–1026, 2007.

[2] W. Kohn and L.J. Sham. Self-consistent equations including exchange and correlation effects. *Phys. Rev.*, 140(4A):1133–1138, 1965.

[3] Gregory H. Wannier. The structure of electronic excitation levels in insulating crystals. *Phys. Rev.*, 52(3):191–197, Aug 1937.

[4] W. E and J. Lu. The continuum limit and quasi-continuum approximation of quantum mechanics models for crystalline solids. *Commun. Math. Sci.*, 5(3):679–696, 2007.

[5] F. Mauri, G. Galli, and R. Car. Orbital formulation for electronic-structure calculations with linear system-size scaling. *Phys. Rev. B*, 47(15):9973–9976, Apr 1993.

[6] C.J. García-Cervera, Jianfeng Lu, Yulin Xuan, and Weinan E. A linear scaling subspace iteration algorithm with optimally localized non-orthogonal wave functions for kohn-sham density functional theory. *Phys. Rev. B*, 79(11):115110, 2009.

Force-based atomistic/continuum hybrid models

Christoph Ortner

(joint work with Matthew Dobson, Mitchell Luskin, Endre Süli)

The motivation for multiphysics coupling methods is that the accuracy of a fine scale model is often only needed in localized regions of the computational domain, but only through a course-grained model can the simulation of large enough systems to include long-range effects be achieved. Despite several creative attempts [1, 2], significant obstacles remain to the development of efficient and accurate hybrid coupling energies. The force-based approach has become very popular because it provides a simple and efficient method for coupling two physics models without the development of a consistent coupling energy: the equilibrium equations at each degree of freedom are obtained from one of the physics models.

In this talk, which is based on the preprints [3, 4], and on ongoing work with E. Süli [6], I discuss the unusual stability properties of the force-based quasicontinuum (QCF) approximation, in the simplest possible setting.

Consider a simple atomistic energy functional

$$\mathcal{E}(y) = \varepsilon \sum_{\ell=-N+1}^{N} \big[\phi(y'_\ell) + \phi(y'_\ell + y'_{\ell+1}) - f_\ell y_\ell\big],$$

where the displacement $u = y - x$ ($x = (x_\ell) = (\varepsilon\ell)$) is $2N$-periodic and has zero mean, $\varepsilon = 1/N$, and $y'_\ell = \varepsilon^{-1}(y_\ell - y_{\ell-1})$. The *local QC approximation* of $\mathcal{E}$ is the short-ranged functional

$$\mathcal{E}^c(y) = \varepsilon \sum_{\ell=-N+1}^{N} \big[\phi(y'_\ell) + \phi(2y'_\ell) - f_\ell y_\ell\big].$$

Thus, a non-local second neighbour interaction is replaced by a local nearest-neighbour interaction, which subsequently makes it possible to remove degrees of freedom for an efficient computational algorithm.

The QCF operator is defined as

$$\mathcal{F}_\ell(y) = \begin{cases} -\frac{1}{\varepsilon}\frac{\partial \mathcal{E}(y)}{\partial y_\ell}, & \ell = -K, \dots, K, \\ -\frac{1}{\varepsilon}\frac{\partial \mathcal{E}^c(y)}{\partial y_\ell}, & \text{otherwise,} \end{cases}$$

where the index set $\{-K, \dots, K\}$ is the *atomistic region*. A linearization about the reference state x leads to the linear system

$$Lu = f,$$

where

$$(Lu)_\ell = \phi''(1)\frac{-u_{\ell+1} + 2u_\ell - u_{\ell-1}}{\varepsilon^2} + 4\phi''(2)\begin{cases} \frac{-u_{\ell+2}+2u_\ell-u_{\ell-2}}{4\varepsilon^2}, & \ell = -K, \dots, K, \\ \frac{-u_{\ell+1}+2u_\ell-u_{\ell-1}}{\varepsilon^2}, & \text{otherwise.} \end{cases}$$

The linearized QCF operator L, especially its stability properties, was the subject of detailed studies in [3, 4].

We begin by noting that the hessians of $\mathcal{E}$ and $\mathcal{E}^c$ at the reference state x are positive definite, uniformly as $N \to \infty$, if and only if $\phi''(1) + 4\phi''(2) > 0$. Thus, the natural question is whether the QCF operator inherits this property. The answer is unfortunately negatory. As a matter of fact, it is shown in [3, 4] that, if $\phi''(2) \neq 0$, then

$$\inf_{\|u'\|_{\ell^2_\varepsilon}=1} \langle Lu, u\rangle \sim -N^{1/2} \quad \text{as } N \to \infty.$$

Moreover, if we try to directly establish operator stability of L in discrete Sobolev spaces $\mathcal{U}^{k,p}$, which are natural variants of the usual Sobolev spaces $W^{k,p}$, then we find that

$$\|L\|_{\mathcal{L}(\mathcal{U}^{1,p},\mathcal{U}^{-1,p})} \sim N^{1/p} \quad \text{as } N \to \infty,$$

that is, L is not uniformly stable in $\mathcal{U}^{1,p}$, in the system size. These results warrant significant doubt regarding the stability and accuracy of the QCF method, and they pose particular challenges for the development of iterative solution methods [5].

While we were able to prove stronger stability results in the spaces $\mathcal{U}^{1,\infty}$ and $\mathcal{U}^{2,\infty}$, leading to optimal error estimates, due to the nature of these spaces, it is highly unlikely that results of this type can be generalized to application relevant 2D and 3D models.

In response to this situation, a stabilization procedure for the QCF equations is proposed in [6]. By identifying the precise origin of the instability, a variational variant of the QCF equations,

$$\langle L^s u, v\rangle := \langle Lu, v\rangle + \alpha\varepsilon\langle u'', v''\rangle_{\mathcal{I}} = \langle f, v\rangle \qquad \forall v,$$

where α is a stabilization parameter, and $\langle\cdot,\cdot\rangle_{\mathcal{I}}$ denotes an inner product over a suitably chosen interface region. For this stabilized method, we obtain the following result:

$$\inf_{\|u'\|_{\ell^2_\varepsilon}=1} \langle L^s u, v\rangle \geq \phi''(1) + 4\phi''(2) - \frac{C}{\alpha}.$$

A generalization of these ideas to fully nonlinear models and higher dimensions is in progress [6].

References

[1] T. Shimokawa, J. Mortensen, J. Schiotz, and K. Jacobsen, *Matching conditions in the quasicontinuum method: Removal of the error introduced at the interface between the coarse-grained and fully atomistic region*, Phys. Rev. B, **69**(21):214104 (2004).

[2] W. E, J. Lu, and J. Yang, *Uniform accuracy of the quasicontinuum method*, Phys. Rev. B, **74**(21):214115 (2004).

[3] M. Dobson, M. Luskin, and C. Ortner, *Sharp stability estimates for the force-based quasicontinuum method*, arXiv:0907.3861 (2009).

[4] M. Dobson, M. Luskin, and C. Ortner, *Stability, instability, and error of the force-based quasicontinuum approximation*, arXiv:0903.0610 (2008); to appear in Arch. for Rat. Mech. Anal..

[5] M. Dobson, M. Luskin, and C. Ortner, *Iterative methods for the force-based quasicontinuum approximation*, in progress.

[6] C. Ortner, and E. Süli, *Stabilized force-based quasicontinuum methods*, in progress.

Viscous flow with moving triple point

Hans Knüpfer
(joint work with Nader Masmoudi)

We consider the spreading of a thin-liquid viscous droplet on a plate. At the triple point where air and liquid meet the solid substrate, the liquid assumes a constant, non–zero contact angle (*partial wetting*). For the case of a Darcy flow, we show well–posedness of this free boundary problem describing the evolution of the free boundary and the velocity of this co–dimension two boundary where air–liquid and solid intersect. In the limit of thin films, the so called *lubrication approximation* regime, we show convergence to the solution of a one-dimensional model, the so called *thin–film equation (TFE)*. Two–dimensional Darcy flows describe the flow through porous media and the flow between the plates of a Hele–Shaw cell (the supporting plate in this case describes a barrier between the plates of the cell). We also consider the Darcy flow as model problem for the Stokes flow which is work in progress.

We first introduce the Darcy flow: Consider a fluid described by its velocity $u = (v, w)$ in Eulerian coordinates. The region occupied by the liquid is described by its height profile $h(t, x)$. The usual kinetic conditions hold: Mass conservation $\nabla \cdot u = 0$, the motion of the free boundary equals the normal velocity V of the liquid. Furthermore, the following dynamic conditions are satisfied: The velocity is given by the gradient of the pressure p. Furthermore, the pressure equals the curvature κ at the air–liquid interface. At the moving triple point, the contact angle is determined by the balance between the surface tension of air, liquid and solid. We are interested in the case of small contact angles of order ϵ. We get:

$$\begin{cases} u = -\nabla p, \quad \nabla \cdot u = 0 & \text{for } 0 < y < h(t,x) \\ p = \kappa, V = u \cdot \nu & \text{for } y = h(t,x) \\ p_y = 0 & \text{for } y = 0 \\ h_x = \epsilon, \quad \dot{s}(t) = -p_x & \text{at } \partial\{h > 0\} \times \{0\}. \end{cases}$$

The first lubrication approximation on the basis of formal asymptotics has been introduced already in 1886 by Reynolds [10]. He formally derives a reduced TFE from the Stokes flow. The corresponding reduced model for the Darcy flow, the TFE with linear mobility, is given by

$$\begin{cases} h_t + (h\ h_{xxx})_x = 0 & \text{in } \{h > 0\} \\ h = 0, \quad h_x = 1, \quad \dot{s}(t) = h_{xxx} & \text{at } \partial\{h > 0\}. \end{cases}$$

In the following, we present our main results and also give a brief review on related analysis. We first consider the blow–up situtation near a (say left) moving triple point. In this case, the initial data approximate the infinite cone with opening angle ϵ. The problem can then be transformed to a nonlocal evolution equation on the half-space $\mathbb{R}_+ := [0, \infty)$. The evolution is described in terms of the single unknown $\epsilon f(t, x) := \partial_x h(t, x - s(t))$ where $s(t)$ is the movement of the triple

point. Our analysis is based on weighted Sobolev norms on $\mathbb{R}_+$. For every $j \in \mathbb{N}$, let $[f]^2_{W^{j,\beta}} := \int_0^\infty r^{2\beta} |\partial_x^j f|^2 \, dx$. The solution f is controlled in terms of:

$$\|f\|_{X^k_\epsilon} := \|f\|_{X^k_{\epsilon,+} + \epsilon^k X^k_{\epsilon,-}} = \inf_{f=f_- + f_+} \big(\|f_+\|_{X^k_{\epsilon,+}} + \frac{1}{\epsilon^k} \|f_-\|_{X^k_{\epsilon,-}} \big),$$

$$\text{where} \qquad \|f\|^2_{X^k_{\epsilon,+}} := \sum_{\ell=0}^k [f]^2_{W^{4\ell,\ell}}, \qquad \|f\|^2_{X^k_{\epsilon,-}} := \sum_{\ell=0}^k [f]^2_{W^{3\ell,0}}.$$

The above norms describe the transition from a operator of third order (Darcy flow) to a fourth order operator (TFE) in the limit $\epsilon \to 0$. Corresponding norms $\| \cdot \|_{Y^k}$ for the pressure are also defined. Our first main result is well-posedness and uniform bounds for the Darcy flow:

Theorem 0.1 (Existence, uniqueness, uniform bounds for Darcy)**.** *Let k be sufficiently large. Let $\|f_0\|_{X^k_\epsilon} \leq \alpha$ for some (small) universal $\alpha > 0$ satisfying some compatibility condition. Then there is a unique global in time solution f of the (transformed) Darcy flow with initial data f_0. Uniformly in ϵ, we have*

$$\sum_{i+j=k+1} \|f\|_{H^i(X^j_\epsilon)} \leq C\alpha \, \|f_0\|_{X^k_\epsilon}.$$

The pressure is also uniformly controlled

$$\|p_\epsilon \circ \Psi\|_{L^2(Y^{k+1})} \leq C\alpha \, \|f_0\|_{X^k_\epsilon},$$

where Ψ_ϵ is some uniformly controlled pull–back on the fixed domain.

We only know about one previous result on well–posedness of (non–stationary) evolution of a fluid on a non–smooth domain. In [2], well–posedness of the Darcy flow is shown. However, the result is based on stronger regularity assumptions on the initial data than we need. In particular, their assumptions exclude the movement of the triple point (and hence propagation of the droplet). Furthermore, the analysis in [2] does not include uniform bounds in the limit $\epsilon \to 0$ and hence is not suited for the lubrication approximation.

As a consequence of the uniform bounds in Theorem 0.1, we get convergence of solutions of the Darcy flow to solutions of the TFE. Furthermore, we show that in the limit, we have $p = p(t, x)$ (independent of the vertical direction):

Theorem 0.2 (Convergence from Darcy to TFE)**.** *Suppose that $f_0 \in X^{k+1/2}_\epsilon$ satisfies some compatibility condition and $\|f_0\|_{X^{k+1/2}_\epsilon} \leq \alpha$ for some small universal $\alpha > 0$. Then the corresponding solutions f_ϵ of the (transformed) Darcy flow with initial data f_0 and contact angle ϵ converge to a function f, global solution of the (transformed) TFE with initial data f_0. Furthermore, $p_\epsilon \to p$ where $p = p(t, x)$.*

We also have corresponding short–time existence and convergence results in the case of a droplet as initial data. Convergence of the Darcy flow to the TFE in the framework of weak solutions has been already shown in [1]. The authors show convergence in the supremum norm to a weak solution of the thin–film equation. In contrary to our result, the analysis in [1] does not include an existence proof

for the initial model. Furthermore their solutions are not regular enough to treat the free boundary explicitly. In particular, their analysis cannot be extended to the case of non–zero contact angle.

We also prove existence and regularity for classical solutions of the TFE:

Theorem 0.3 (Existence, regularity & uniqueness for TFE)**.** *Let k be sufficiently large. Suppose that $f_0 \in X_0^{k+1/2}$ satisfies some compatibility condition and furthermore $\|f_0\|_{X_0^k} \leq \alpha$ for some (small) universal $\alpha > 0$. Then there is a unique global in time solution f of the (transformed) TFE with initial data f_0. We have*

$$\sum_{i+j=k+1} \|f\|_{H^i(X_0^j)} \;\leq\; C\alpha \; \|f_0\|_{X_0^{k+1/2}}.$$

Existence results on the TFE with zero contact angle are well established: Existence of weak solutions has been shown in [12, 9, 11], uniqueness of weak solutions is unknown. Existence and uniqueness of classical solutions has been shown in [8]. All the above results address the case where the liquid attains a zero contact angle at the triple point. There is only one result for the partial wetting regime where existence (but not uniqueness) of weak solutions is proved [13]. Hence, this is the first existence and uniqueness result for classical solutions of the TFE with non–zero contact angle.

References

[1] L. Giacomelli and F. Otto, *Rigorous lubrication approximation*, Interfaces free Boundary **5** (2003), 483–529.

[2] B. Bazalyi and A. Friedman, *The Hele-Shaw problem with surface tension in a half-plane: a model problem*, J. Diff. Eq **216** (2005), 387–438.

[3] B. Bazalyi and A. Friedman, *The Hele-Shaw problem with surface tension in a half-plane*, J. Diff. Eq **216** (2005), 439–469.

[4] G. Prokert, *Existence results for Hele-Shaw flow driven by surface tension*, Eur. J. Appl. Math. **9** (1998), 195–221.

[5] J. Escher and G. Simonett, *Classical solutions for the quasi-stationary Stefan problem with surface tension*, Math. Res. Akademie Verlag, **100** (1997), 98–104.

[6] J. Escher and G. Simonett, *Classical solutions for Hele-Shaw models with surface tension*, Adv. Diff. Eq., **2** (1997), 619–642.

[7] P. Constantin and M. Pugh, *Global solutions for small data to the Hele-Shaw problem*, Nonlinearity, **6** (1993), 393–415.

[8] L. Giacomelli, H. Knüpfer and F. Otto, *Smooth zero-contact-angle solutions to a thin-film equation around the steady state*, J. Diff. Eq., **245** (2008), 393–415.

[9] E. Beretta,R. Dal Passo and M. Bertsch, *Nonnegative solutions of a fourth-order nonlinear degenerate parabolic equation*, Arch. Rat. Mech. Anal., **129** (1995), 175–200.

[10] O. Reynolds, *On the Theory of Lubrication and Its Application to Mr. Beauchamp Tower's Experiments, Including an Experimental Determination of the Viscosity of Olive Oil*, Proc. Royal Soc. of London, **40** (1886), 191–203.

[11] A. Bertozzi and M. Pugh, *The lubrication approximation for thin viscous films: regularity and long-time behavior of weak solutions*, CPAM, **49** (1996), 85–123.

[12] F. Bernis and A. Friedman, *Higher order nonlinear degenerate parabolic equations*, JDE, **83** (1990), 179–2006.

[13] F. Otto, *Lubrication approximation with prescribed nonzero contact angle*, CPDE, **23** (1998), 2077–2164.

Influence of driving mechanism on avalanche criticality in first-order phase transitions

Antoni Planes
(joint work with D. Soto-Parra, E. Vives, L. Mañosa and R. Romero)

Many ferroic and multiferroic materials undergo first-order phase transitions which occur through a sequence of discontinuous steps or avalanches of the order parameter. These avalanches are acknowledged to reflect the fact that, when slowly driven, these systems relax from a (marginally stable) metastable state towards another metastable state with associated energy dissipation responsible for hysteresis. Usually, since metastable minima are separated by very high energy barriers, the transition kinetics is not dominated by thermal fluctuations (athermal behaviour). The configuration of metastable minima is determined by the intrinsic distribution of disorder in the system. This yields a complex free-energy landscape that is at the origin of the noisy nature of the response to the driving field and of mesoscale phase separation reflected in a complex multidomain structure [1]. Martensitic materials are typical examples of this class of systems. In these ferroelastic materials avalanches are related to sudden changes in the local strain field which give rise to the emission of high-frequency acoustic waves. This is the so-called acoustic emission (AE) [2] which is the analogue of Barkhausen noise in magnetic materials (associated with sudden changes of the local magnetization) [3]. In addition to magnetic and structural systems, a similar phenomenology has been reported in systems such as ferroelectrics [4] and superconductors [5, 6]. In all these materials, the distributions of size and duration of the avalanches often display power law behaviour which reveals a tendency to reach a critical point characterized by the absence of size and time scales [7]. Models accounting for avalanche criticality assume some kind of interplay between disorder and transition variables and field-driven athermal dynamics. These models can be classified into the following two general classes [3]; lattice models of the random-field Ising type and domain wall models. In the former case, nucleation regimes dominate and critical behaviour requires fine tuning of the amount of disorder. In the second class, criticality is related to a pinning-depinning transition and fine tuning of disorder is not required. Therefore, classical order-disorder criticality is predicted in the first case, while self-organized criticality is expected to occur in domain wall models.

The driving mechanism has been argued to strongly influence avalanche criticality. The two important extreme driving situations consist of controlling either the externally applied field or its corresponding generalized displacement (thermodynamically conjugated variable). In the first case, driving is soft in the sense that displacement is free to fluctuate, while it is hard in the second case since displacement is constrained by the driving device [8, 9, 10]. Recently, this problem has been theoretically addressed by Pérez-Reche et al. [11] who predicted a crossover from classical to self-organized criticality when moving from soft- to hard-driving.

From an experimental point of view, reliable control of the generalized displacement (i.e., magnetization in magnetic systems or polarization in ferroelectrics) in the transition region where systems display non-linear behaviour is difficult. Commonly, the field is the variable which is easy to control (soft-driving), while it is difficult to induce the transition by controlling the corresponding conjugated displacement (hard-driving), as it needs a complicated feedback mechanism. In systems undergoing structural transitions, where a component of the strain tensor is the order parameter, the two conjugated variables are strain and stress which are respectively related to the elongation of the system and the applied force. Since it is quite easy to control both force and elongation, we have decided to analyse the effect of driving mechanism on avalanche criticality in the case of a structural transition by comparing results in force-controlled (soft) and elongation-controlled (hard) conditions. We have used a standard (screw-driven) tensile machine for hard-driven experiments and a specially designed machine [10] that enables an increasing/decreasing dead load (force) hanging from the sample to be controlled for soft-driven experiments. The same sample, grips, strain gauge and load cell were used in both driving devices. In both cases, avalanches were quantified from the AE generated during the martensitic transition. The studied sample was a $Cu_{68.13}Zn_{15.74}Al_{16.13}$ single crystal that exhibits a cubic ($L2_1$) to monoclinic (18R) transition. The sample has cylindrical heads and a 35 mm (long) $\times$ 1.4 mm $\times$ 3.95 mm body. Prior to the sequences of load-unload cycles performed in soft- and hard-driven modes, an appropriate heat treatment was performed so that the sample was in the ordered state, free from internal stresses and the vacancy concentration was a minimum at room temperature (clean sample).

The following results were obtained. (i) The distributions of amplitude and energy of the avalanches show power law behaviour in both soft- and hard-driving experiments. (ii) In the case of soft-driving, when starting with a clean sample, the exponents that characterize the amplitude and energy distributions evolves during transition cycling and tend to stabilize after a given number of cycles (about 7 cycles). (iii) Instead, within the experimental error, no evolution occurs in similar hard-driven experiments. Since it is well known that disorder (in the form of dislocations) increases during cycling with a tendency to reach saturation after a few cycles [12], the evolution of the critical exponents in soft-driven experiments is consistent with the prediction [11] that fine tuning of the amount of disorder is needed in order to reach criticality, while it is not needed in hard-driven experiments (where no evolution of the exponents is detected). The fact that exponents (in the stationary regime) are larger for soft-driving than for hard-driving is also in agreement with these theoretical predictions. It is worth noticing that quantitative comparison of experimental exponents with theoretical estimation is difficult since it is not yet clear what the exact relation is between the energy and amplitude of AE signals and the energy released, size or duration of the avalanches.

References

[1] T. Castán, Ll. Mañosa, E. Vives, A. Planes, and A. Saxena, in *Magnetism and Structure in Functional Materials* ed. by A. Planes, Ll. Mañosa, and A. Saxena, Springer Verlag, Berlin, 2005, pp. 27-48.

[2] C.B.Scruby, *An introduction to acoustic-emission*, J.Phy. E:Sci.Instrum. **20**, 946 (1987).

[3] G. Durin and S Zapperi, in *The Science of Hysteresis* ed. by G. Bertotti and I.D. Mayergoyz, Elesvier, Amsterdam, 2005, Vol. II, pp. 130-267.

[4] M. Roth, E. Mojaev, E. Dulkin, P. Gemeiner, and B. Dkhil, *Phase transition at a nanometer scale detected by acoustic emission within the cubic phase* Pb(Zn1/3Nb2/3)O-3-xPbTiO(3) *relaxor ferroelectrics* Phys. Rev. Lett. **98**, 265701 (2007).

[5] W.Wu and P.W. Adams, *Avalanches and slow relaxation-dynamics of ultrathin granular superconducting films in a parallel magnetic-field* Phys. Rev. Lett. **74**, 610 (1995)

[6] S. Field, J. Witt, F. Nori and X. Ling, *Superconducting vortex avalanches* Phys. Rev. Lett. 74, 1206 (1995).

[7] J. P. Sethna, K. A. Dahmen, and C. R. Myers, *Crackling noise* Nature **410**, 242 (2001).

[8] G. Puglisi and L. Truskinovsky, *Mechanics of a discrete chain with bi-stable elements* J. Mech. Phys. Solids **48**, 1 (2000).

[9] X.Illa, M.L.Rosinberg and E.Vives, *Influence of the driving mechanism on the response of systems with athermal dynamics: The example of the random-field Ising model* Phys. Rev. B **74**, 224403 (2006); X.Illa, M.L.Rosinberg, P.Shukla and E.Vives, *Magnetization-driven random-field Ising model at T=0* Phys. Rev. B **74**, 224404 (2006).

[10] E.Bonnot, R.Romero, X.Illa, Ll.Mañosa, A.Planes and E.Vives, *Hysteresis in a system driven by either generalized force or displacement variables: Martensitic phase transition in single-crystalline Cu-Zn-Al* Phys. Rev. B 76, 064105 (2007).

[11] F. J. Pérez-Reche, L. Truskinovsky and G. Zanzotto, *Driving-Induced Crossover: From Classical Criticality to Self-Organized Criticality* Phys. Rev. Lett. **101**, 230601 (2008).

[12] F.J. Pérez-Reche, M. Stipcich, E. Vives, Ll. Mañosa, A. Planes, and M. Morin, *Kinetics of martensitic transitions in Cu-Al-Mn under thermal cycling: Analysis at multiple length scales* Phys. Rev. B **69**, 064101 (2004).

Elastic free energies, lattice based Hamiltonians, and gradient Gibbs-Young measures

Stephan Luckhaus

(joint work with R. Kotecký)

The aim is to give a description of elastic behaviour in the framework of positive temperature equilibrium mechanics. This means that we start from a lattice based particle model with an interaction potential U that is invariant under rigid motion. For this potential we define the finite volume Gibbs measure, with clamped boundary conditions, and under rescaling we look at the two scale limit of this measure.

In this way we try to capture at the same time the macroscopic behaviour of the rescaled function and the local picture of relative positions of particles in the lattice. What results is a gradient Gibbs measure $\mu_{x,v}$ parametrized over the macroscopic Lagrangian variable x and the possible macroscopic deformation v. The possible deformations v are minimizers of a stored energy functional $\int W(\nabla v)$ which, in statistical mechanics terms, is the large deviation rate functional of the theory. The expected strain under $\mu_{x,v}$ is $\nabla v(x)$.

To be more precise, the particle configurations are

$$X : \mathbb{Z}^d \cap \tfrac{1}{\epsilon}\Omega \to \mathbb{R}^m,$$

the potential is given as

$$U : (\mathbb{R}^m)^A \to \mathbb{R}, \text{ where } A \subset \mathbb{Z}^d \text{ is finite,}$$

and the Hamiltonian is

$$H(X|u) = \sum_{j \in \mathbb{Z}^d \cap \frac{1}{\epsilon}\Omega} U(X_u|_{A+j})$$

where

$$X_u(i) = \begin{cases} X(i) \text{ for } \epsilon i \in \Omega \\ \frac{1}{\epsilon} u(\epsilon i) \text{ otherwise.} \end{cases}$$

The scaling is such that it leaves the gradient invariant, which is the reason why we end up with the first order elasticity theory.

In this context and supposing, e.g., that U fulfils the assumption

$$\frac{1}{c} \sum_{j\,:\,|j|=1} |X(0) - X(j)|^p - N \le U(X_A) \le c \sum_{j\,:\,|j|=1} |X(0) - X(j)|^p + N,$$

we can show that there exists a free energy

$$-W(L) = \lim_{\epsilon \to 0} \frac{\epsilon^d}{\beta|\Omega|} \log\Big(\int \exp\big\{-\beta H(X|u_L)\big\} \prod_{i \in \mathbb{Z}^d \cap \frac{1}{\epsilon}\Omega} dX(i) \Big),$$

where $u_L(x) = Lx$ with a linear map L.

If one looks at any reasonable interpolation $\Pi_\epsilon(X)$ of $\epsilon X(\lfloor \frac{x}{\epsilon} \rfloor)$, then the two scale convergence of the measure

$$\mu_\epsilon(M) = \frac{1}{Z} \int_M \exp\big\{-\beta H(X|u)\big\} \prod_{i \in \mathbb{Z}^d \cap \frac{1}{\epsilon}\Omega} dX(i),$$

where Z is the normalising constant, is described via the cylinder test functions

$$\varphi(X, v, x) = \tilde{\varphi}(X_{i_1}, \dots, X_{i_k}, \alpha_1^{(v)}, \dots, \alpha_k^{(v)}, x)$$

where $\tilde{\varphi}$ is continuous with at most linear growth and $\alpha_\ell^{(v)} \in H_p^{-1}$. For these test functions, one has

$$\int \varphi(X(\cdot + \lfloor \tfrac{x}{\epsilon} \rfloor), \Pi_\epsilon(X), x) d\mu_\epsilon \to \int_C \int_\Omega \int_{(\mathbb{R}^m)^{\mathbb{Z}^d}} \varphi(X, v, x) d\mu_{x,v}(X) d\gamma(v) dx.$$

Here, $\mu_{x,v}$ is a Gibbs measure (on gradients), γ is a probability measure on the weakly compact set $C = \{v \in u + \overset{0}{H}{}_p^1 \mid \int W(\nabla v) = \min\}$ (i.e. a Radon measure on this set equipped with weak topology).

Crucial tools are the following observations:

1. *Exponential tightness:*

$$\mu_\epsilon(\{X \mid H(X) > K\}) \le \exp(-cK\epsilon^{-d}) \text{ for } K \text{ large.}$$

2. *Equivalence of free energies:*

$$\lim \epsilon^d \log\log Z_{\frac{1}{\epsilon}\Omega,u_L} = \lim_{\kappa\to 0}\lim_{\epsilon\to 0} \epsilon^d \log Z_{\frac{1}{\epsilon}\Omega}(\mathcal{N}_p(u_L,\kappa)),$$

where $Z_{\Lambda,u_L} = \int \exp(-\beta H(X|u_L)) \prod_{i\in\Lambda} dX(i)$, and

$$Z_\Lambda(\mathcal{N}_p(u_L,\kappa)) = \int_{\mathcal{N}_p(u_L,\kappa)} \exp(-\beta H(X)) \prod_{i\in\Lambda} dX(i)$$

with $\mathcal{N}_p(u_L,\kappa) = \{X \mid \int |u_L - \Pi_\epsilon(X)|^p < \kappa\}$ (and $H(X) = \sum_{j+A\subset\frac{1}{\epsilon}\Omega} U(X|_{j+A})$).

The second claim is proved via an interpolation lemma for the Gibbs measure with different boundary conditions.

Challenges in modelling TCP formation in Ni-based superalloys

Ralf Drautz

(joint work with Bernhard Seiser, Thomas Hammerschmidt, David G. Pettifor)

Refractory elements like Re and W are added to Ni-based superalloys to improve the creep resistance of the alloys. It is observed that too large concentrations of refractory elements induce the formation of topologically close-packed (TCP) phases.

The TCP phases destroy the single crystalline lattice of the Ni-based superalloys and are detrimental to the mechanical properties of the alloy. Empirical models that aim to predict the formation of TCP phases as a function of the average valence electron count are found to be not reliable.

We use analytic bond-order potentials [1] to predict the stability of TCP phases. The bond-order potentials are derived through coarse-graining the electronic structure at two levels of approximation. First, the Kohn-Sham equations of density-functional theory are simplified to the tight-binding bond model by using a minimal basis set of atomic-like orbitals and by parametizing the Hamiltonian matrix-elements using analytic functions and the two-centre approximation. The total energy within density-functional theory is further approximated by its second-order expansion with respect to charge fluctuations.

Second, using the moments theorem that relates the crystal structure to the electronic density of states, analytic interatomic bond-order potentials are obtained by expanding the density of states in terms of response functions that only depend on the Fermi energy and moments of the density of states that are given as functions of the local atomic environment.

With the help of the analytic bond-order potentials the structural stability of TCP phases is then characterized as a function of the number of valence electrons and the lattice structure. For example, at the fourth moment level we observe a distinct separation of the TCP phases in two groups, (σ, A15, χ) and (μ, Laves phases). The μ phase and the Laves phases are stabilized by the size differences of the constituent atoms, while the A15, σ and χ phases are stablilized by the average electron count even if the constituent atoms are of similiar size.

Based on the analysis of the stability of the TCP phases as a function of size difference and valence electron count, we propose a new, 2-dimensional structure map. We hope that the new structure map will be useful for alloy developers for guiding the design of new alloys.

References

[1] R. Drautz and D.G. Pettifor, *Valence-dependent analytic bond-order potential for transition metals*, Phys. Rev. B**74** (2006), 174117.

Domain boundary engineering

Ekhard Salje

We review the idea that domain boundaries, rather than domains, can carry information and act as memory devices. Domains are bulk objects; their large response to changing external fields is related to their change in volume, which implies the movement of domain boundaries. In many cases, the design of 'optimal' domain structures corresponds to 'optimal' domain boundaries with parameters such as the domain boundary mobility, pinning properties and the formation of specific boundaries such as curved boundaries or needle domains. This argument is enhanced further in this review: domain boundaries themselves can host properties which are absent in the bulk, they can be multiferroic, superor semi-conductors while the matrix shows none of these properties. It is agued that multiferroic walls can be described formally as chiral whereby the chirality relates to state-vectors such as polarisation and magnetic moment and their (non-linear) coupling. Once such walls can be generated reliably, a new generation of devices with much higher storage density than ever produced before can be envisaged.

Before we investigate the intrinsic changes of the crystal structure inside twin walls, we focus on their chemical modifications. Chemical transport along twin walls and grain boundaries is well understood to be different from that of the bulk. In general, transport is faster along twin walls (or grain boundaries) so that any modification of the twin wall composition is relatively easily achieved when the sample is exposed to external chemical agents. These can then diffuse and equilibrate along the walls while the bulk remains relatively unaffected. In material sciences of ferroic materials we have examples where small amounts of Na were injected into WO_3. As a result, the composition of the twin walls changed from WO_3 to Na_xWO_3 or WO_{3-x} which are for certain values of x superconducting phases. Indeed, these twin walls became superconducting while the bulk remained an insulator.

It is important to note that transport can also be reduced in twin walls for specific materials. Such a case is related to the transport of Na and Li through a quartz crystal with {100} Dauphine twinning. Computer simulation showed that the transport rate along the twin walls was reduced for the [0 0 1] channels. This effect is related to the local structure of quartz at the twin boundary; structural continuity across the twin boundary requires that the [0 0 1] channels are

more distorted in the twin wall than in the bulk material while the volume of the channels increases. This increase goes together with a decrease of the minimum diameter of the channels which, ultimately, limits the transport. The probably most common doping in perovskite oxides relates to oxygen vacancies. Significant pinning of the movement of twin boundaries by oxygen vacancies occurs in polycrystalline $Ca_{1-x}Sr_xTiO_3$ and $LaAlO_3$ single crystals. The activation energy for domain wall motion (determined from the temperature and frequency dependence of the storage modulus and loss tangent), is of the order of $0.88 - 1.09$ eV, which is comparable with the activation energy for O-atom diffusion through a perovskite structure. The accumulation of defects influences the thickness of the domain.
Before we discuss the modification of twin walls when two order parameters interact, we recur to a recent study Goncalves-Ferreira et al. [1]. These authors explored the idea that all TiO_6-based perovskite structure may have a tendency to possess polar walls even when the bulk of the material is non-polar. The fundamental idea relates simply to the instability of Ti inside any oxygen octahedron of sufficient size to remain in the centre of the octahedron. It is easy to visualise that an energy minimum exists in such structures in which Ti forms bonds with a subset of oxygen atoms at the expense of the remaining atoms. If Ti forms a bond with one oxygen atom the octahedron suffers tetragonal deformation. Equivalently, bonding with 2 (3) oxygen would lead to an orthorhombic (trigonal) deformation. In a structure this tendency can be compensated by the next nearest neighbour interactions and, while the details of the force balance for Ti can be complex, it may lead to a high symmetry phase at high temperatures.

In domain walls, on the other hand, such constraints are limited because the local symmetry is broken anyway and new secondary order parameters become possible. This scenario goes beyond the order parameter/strain coupling as discussed so far and requires two structural instabilities which couple according to their respective symmetry rules. This coupling is best visualised in the so-called order parameter vector space which has been used for several cases. A convenient way to depicture such mixed state of multiferroics or degenerate order parameter is to construct the order parameter vector space [2]. In this construction, each state parameter defines a subspace of dimension n (the degeneracy of the order parameter, i.e. the dimensionality of the active representation) in which this state is described. Fig.2 (below) shows results of numerical studies of the off-centering of Ti in octahedral coordination from the centre of symmetry and the compressibility of the unit cell as represented by the distance between two Ti positions. The lower curve represents the bulk, the upper curve shows the domain wall. The domain wall is widenend with larger units cells and slightly more compressible.

References

[1] L. Goncalves-Ferreira, S.A.T. Redfern, E. Artacho, E.K.H. Salje, *Ferrielectric Twin Walls in $CaTiO_3$*, Phys. Rev. Letters **101(9)** (2008), Article Number: 097602

[2] E.K.H. Salje, *Ferroelastic and Co-elastic Crystals*, Cambridge University Press, Cambridge (1993).

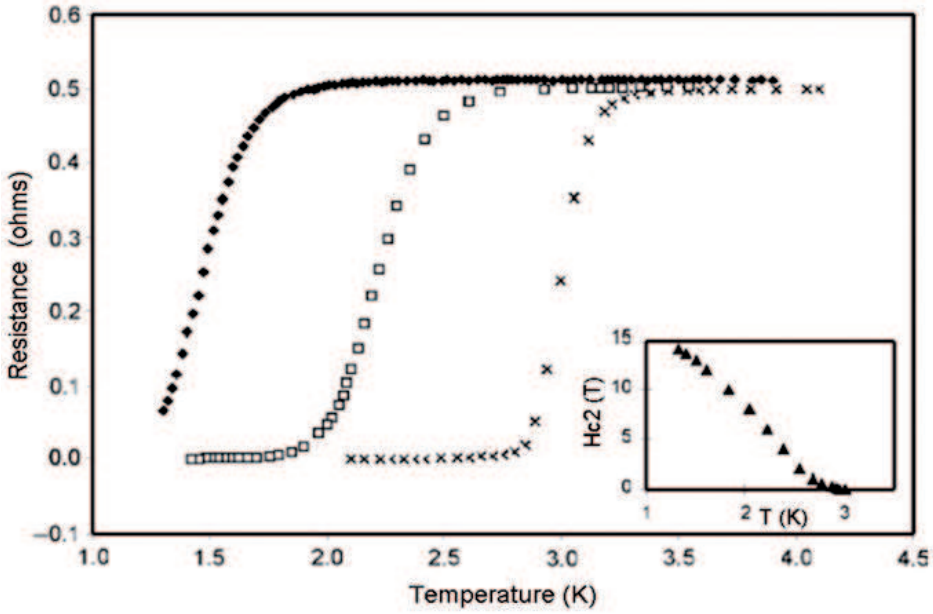

FIGURE 1. Resistivity of a twinned crystal of WO_3 as measured along a twin wall over an extended temperature interval. The onset of superconductivity in the walls is at 3.2 K. The magnetic fields are 0T (crosses), 6T (open squares) and 13T (filled diamonds). The inset shows the temperature dependence of H_{c2}.

Finite temperature coarse-graining of atomistic models: some simple cases

FRÉDÉRIC LEGOLL

(joint work with Xavier Blanc, Claude Le Bris and Carsten Patz)

In this work, we consider atomistic models for materials at constant finite temperature, in a one-dimensional setting. Our aim is to derive a reduced model providing the macroscopic constitutive law relating strain and stress. Building on standard asymptotic tools of probability (such as Large Deviations Principles), we design an efficient, and apparently new, computational strategy.

Consider an atomistic system consisting of N particles, at positions $X = \left(X^1, \ldots, X^N\right) \in \mathbb{R}^N$. Provide this system with an energy $V(X) = V\left(X^1, \ldots, X^N\right)$ and allow the particles to sample $\mathbb{R}$. The finite temperature thermodynamical properties of the material are obtained from canonical ensemble averages,

$$\langle \Phi \rangle = \frac{\displaystyle\int_{\mathbb{R}^N} \Phi(X)\, \exp(-\beta V(X))\, dX}{\displaystyle\int_{\mathbb{R}^N} \exp(-\beta V(X))\, dX}, \tag{1}$$

where Φ is the observable of interest and β is proportional to the inverse temperature. Computing such canonical averages is a standard task of computational

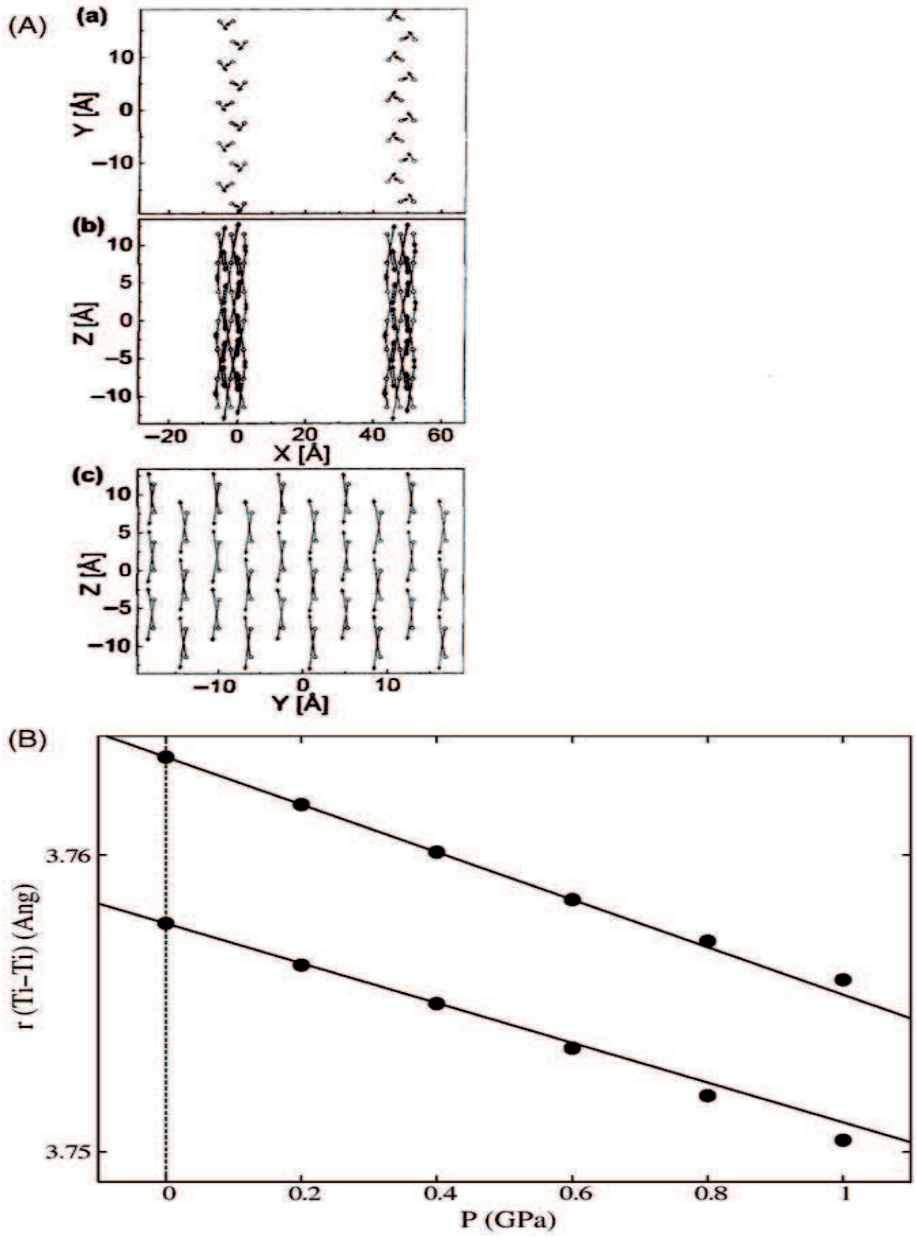

FIGURE 2.

materials science. Of course, the major difficulty comes from the N-fold integral, where N, the number of particles, is extremely large. One possible method is to compute (1) as a long-time average

$$\langle \Phi \rangle = \lim_{T \to +\infty} \frac{1}{T} \int_0^T \Phi(X_t)\, dt \tag{2}$$

along the trajectory generated by the stochastic differential equation

$$dX_t = -\nabla V(X_t)\, dt + \sqrt{2\beta^{-1}}\, dW_t, \tag{3}$$

where W_t is a standard N-dimensional Brownian motion.

It turns out that the derivation of macroscopic constitutive laws is closely related to a seemingly different question, that we describe now. Assume that, in (1), observables of interest do not depend on the positions of *all* the atoms, but only on *some* of them (for instance, because these atoms are located in a region of interest, where some particular phenomenon occurs). We assume that this set of interesting atoms (also called *repatoms*) is given *a priori*, and we denote by X_r their positions. We hence write

$$X = \left(X^1, \dots, X^N\right) = (X_r, X_c), \quad X_r \in \mathbb{R}^{N_r}, \quad X_c \in \mathbb{R}^{N_c}, \quad N = N_r + N_c,$$

and our aim is to compute (1) for such observables, that is

$$\langle \Phi \rangle = Z^{-1} \int_{\mathbb{R}^N} \Phi(X_r) \, \exp(-\beta V(X)) \, dX \tag{4}$$

where $Z = \displaystyle\int_{\mathbb{R}^N} \exp(-\beta V(X)) \, dX$, by a cheaper method than (2)-(3).

Another question of interest concerns the free energy of the reduced system,

$$A(X_r) = -\frac{1}{\beta} \ln \int_{\mathbb{R}^{N_c}} \exp(-\beta V(X_r, X_c)) \, dX_c.$$

When $N_c \to +\infty$, this energy diverges. The meaningful quantity is the free energy per (removed) particle, $A(X_r)/N_c$. Can this quantity be efficiently computed, in the limit $N_c \to +\infty$?

In [1], we have addressed these questions using a thermodynamic limit approach (that is, we consider the limit $N_c \to +\infty$), and we have outlined their link with the derivation of a macroscopic strain-stress relation. We consider the case of next-to-nearest-neighbour interactions:

$$V(X) = \sum_{i=0}^{N-1} U_1\left(\frac{X^{i+1} - X^i}{h}\right) + \sum_{i=0}^{N-2} U_2\left(\frac{X^{i+2} - X^i}{h}\right), \tag{5}$$

where we have rescaled all distances by $h = 1/N$. Here, we focus on the case of a unique repatom, namely the last atom of the chain (generalization to the case of several repatoms is easy). To remove translation invariance, we set $X^0 = 0$.

In that setting, the average (4) reads

$$\langle \Phi \rangle_N = Z^{-1} \int_{\mathbb{R}^N} \Phi(X^N) \, \exp(-\beta V(X)) \, dX, \tag{6}$$

and it turns out that it can be recast as an expectation value:

$$\langle \Phi \rangle_N = \mathbb{E}\left[\Phi\left(\frac{1}{N}\sum_{i=1}^{N} Y_i\right)\right]$$

for random variables Y_i that are a realization of a Markov chain. Hence, using a Law of Large Numbers argument, we can compute a good approximation of the average (6), in the limit $N \to \infty$. In the specific case when $\Phi(X^N) = X^N$, the quantity (6) is nothing else than the **macroscopic elongation of the chain (i.e. strain) for stress-free boundary conditions**.

Assume now that, instead of prescribing stress-free boundary conditions, we prescribe the microscopic strain ℓ (i.e. the elongation of the chain), and that we wish to compute the macroscopic stress. Since this setting is technically more involved than the previous one, we restrict ourselves here to the simple case of nearest-neighbour interactions ($U_2 \equiv 0$ in (5)). For a chain of N atoms, the macroscopic stress is the canonical average of the force between two consecutive atoms:

$$\sigma_N(\ell) = \int_{\mathbb{R}^{N-1}} U_1'\left(\frac{X^{i+1} - X^i}{h}\right)\, d\mu_\ell(X) = \int_{\mathbb{R}^{N-1}} U_1'\left(\frac{\ell - X^{N-1}}{h}\right)\, d\mu_\ell(X),$$

where

$$d\mu_\ell(X) = Z_\ell^{-1} \exp\left(-\beta V\left(X^1, \dots, X^{N-1}, \ell\right)\right)\, dX^1 \dots dX^{N-1}$$

is the canonical measure associated to the system with fixed $X^N = \ell$, and where Z_ℓ is a normalizing constant. We observe here that $\sigma_N(\ell) = A_N'(\ell)$, where A_N is the free energy per removed particle:

$$A_N(X^N) = -\frac{1}{N\beta} \ln \int_{\mathbb{R}^{N-1}} \exp(-\beta V(X^1, \dots, X^N))\, dX^1 \dots dX^{N-1}.$$

Limits of free energies can be handled with classical Large Deviations arguments. We obtain the limit, when $N \to \infty$, of A_N and hence of σ_N, in a closed form amenable to numerical computations.

Note that only the structure of the physical system actually needs to be one-dimensional: the space in which the atoms vary may be $\mathbb{R}^d$, $d \geq 1$. Our strategy hence applies to chain-like systems, such as polymers.

Such an approach may also be considered as a first step toward the numerical analysis of methods commonly used in practice [2], and the assessment of the simplifying assumptions upon which they rely.

References

[1] X. Blanc, C. Le Bris, F. Legoll, C. Patz, *Finite-temperature coarse-graining of one-dimensional models: mathematical analysis and computational approaches*, INRIA preprint RR-6544 (may 2008), available at `http://hal.inria.fr/inria-00282107/en/`.

[2] L. M. Dupuy, E. B. Tadmor, R. E. Miller, R. Phillips, *Finite temperature Quasicontinuum: Molecular dynamics without all the atoms*, Phys. Rev. Lett. **95** (2005), 060202.

Selection in Models for Stage Structured Populations. Example: Alignment.

Angela Stevens

(joint work with Kyungkeun Kang, Benoit Perthame, Ivano Primi, Juan J.L. Velázquez)

1. Introduction

Age structured population models are long established in epidemiology. Often, age and time dynamics are analyzed, less often also space dependencies. We want to explore, if the basic type of mathematical model for stage/age structured populations is also suitable to describe processes of cell differentiation. So far, cell differentiation is mostly modeled hierarchically, e.g. first one 'species' of cells is described and analyzed, then a model for two 'species' is taken into account.

Usually cells vary concerning a specific cellular function e.g. in the developmental cell cycle of the cellular slime mold *Dictyostelium discoideum*. During so-called mound formation, chemotactically more active cells can be found at the top of the mound and chemotactically less active cells at the bottom. Later, these differentially sorted cells differentiate into two cell types, pre-stalk and pre-spore cells.

We suggest the following modeling ansatz. Describe the variability w.r.t. a specific cellular function via a stage parameter, similar to the age parameter in epidemiological models. If the process of cell differentiation is related to this cellular function, then the long time dynamics of the model should select for a finite number of stages from the initial continuum of stages. Thus pre-differentiation can take place.

2. An Example

To get a first insight into the suggested mathematical approach we consider the specific problem of angular alignment of cells and filaments. Examples are myxobacteria and actin filaments. Experimentally the formation of oriented aggregates is observed: for myxobacteria a quasi one-dimensional parallel alignment, [1], and for filaments within the cytoskeleton several oriented bundles. Here, in a first step, we do not focus on problems of cell differentiation, but rather on a phenomenon, where a model with a continuum of stage parameters – here orientation – shows a finite number of stages as long time dynamics. We also want to understand, how orientational aggregation and the final number of oriented bundles depend on the details of cellular interaction.

3. The Model Equations

We consider

$$\partial_t f(t,\gamma) \quad = \quad -\int_I T[f](\gamma,\gamma')f(t,\gamma)d\gamma' + \int_I T[f](\gamma',\gamma)f(t,\gamma')d\gamma'$$

where $T[f](\gamma,\gamma') = \int_I G_\sigma(\gamma'-\gamma-V(w-\gamma))f(t,w)dw$ with $I=[-\frac{1}{2},\frac{1}{2}]$. Here V is the orientational angle, an odd function and 1-periodic, and G_σ measures the accuracy of reorientation and can be chosen as the standard periodic Gaussian.

Bundles of cells or filaments attract each other if they are close in orientation. Depending on the initial distribution, one, two or multiple peaks develop. The shorter the range of optimal turning is, the more likely is the development of many peaks. An example for a k-directional orientational angle is $V(\theta)>0$ in $(0,1/2k), V(\theta)=0$ in $[1/2k,1/2]$.

In the case of myxobacteria if the angle between bacteria is small, they attract each other. If the angle between myxobacteria is larger, they act repulsive, respectively they are attracted to the ends of their interaction partners.

4. Peak Solutions for the Limiting Equation

Consider G_σ with $\sigma = 0$, the Dirac mass δ_0, which describes deterministic turning. Convergence of solutions of our equation for G_σ to solutions for δ_0, for σ small enough, was proved by *E. Geigant*, [2]. Consider a first simple setting for uni-directional alignment: Assume the above mentioned conditions for V and let $suppf_0 = A_1$ with e.g. $A_1 = (-1/4, 1/4)$. Then the first moment of f is preserved

$$\int_I \gamma f(t,\gamma)d\gamma = \int_I \gamma f(0,\gamma)d\gamma \ .$$

The mean of the first moment is

$$\xi = \frac{\int_I \gamma f(t,\gamma)d\gamma}{\int_I f(t,\gamma)d\gamma} \ ,$$

and the following general types of second moments of f are decreasing in time

$$\frac{d}{dt}\int_I (\gamma - \xi)^2 f(t,\gamma)d\gamma \leq 0 \ .$$

Equality only holds in case $f(t,\gamma) = m\delta_{\{\gamma=\xi\}}$. For continuously varying initial distributions an exchange of mass and generalized momenta takes place and the arguments get more involved. In case of attractive and repulsive optimal orientation one has to define suitable partial masses $m_1(t), m_2(t)$ as well as $\xi_1(t), \xi_2(t)$. In [3] it could be proved for initially two slightly asymmetric oriented peaks, that two oriented peaks develop at two exactly opposite orientations $\tilde{\xi}_1, \tilde{\xi}_2$ as long time dynamics. Their final masses $\tilde{m}_1, \tilde{m}_2$ can be different. The initial peaks may differ in size but should both be of higher order of magnitude than the rest of the initial distribution. So we obtained local stability for alignment into two opposite directions, but no selection of mass.

In [4] we had a closer look at the case $\sigma > 0$. If the orientation angle V is very small the kinetic equation can be approximated by

$$\partial_t f = \frac{\sigma^2 m}{2}\partial_{xx} f + \partial_x \left(f(x) \int_I V(x-y) f(y) dy \right) \ .$$

We are interested in the steady states. An equivalent formulation for these is

$$\frac{\sigma^2}{2}\partial_x f(x) + f(x) \int_I V(x-y) f(y) dy = 0$$

$$\int_I f(x)dx = 1 \text{ and } f(x+1) = f(x) \ .$$

5. Heuristics for the Selection Mechanism

Let $\sigma = 0$, then the above equation reduces to

$$f(x) \int_I V(x-y) f(y) dy = 0 \ .$$

Any function of the form $f(x) = \alpha\delta_0(x) + \beta\delta_0(x - \frac{1}{2})$ is a solution, for arbitrary choice of α, β. For $\sigma > 0$ this is not the case. Suppose $f_\sigma \to \alpha\delta_0(x) + \beta\delta_{\frac{1}{2}}(x)$ for $\sigma \to 0$. For $\sigma << 1$, f_σ can then be approximated by the solution of

$$\frac{\sigma^2}{2}\partial_x f(x) + f(x) V_{\alpha,\beta}(x) = 0 \ , \ \int_I f(x) dx = 1$$

where $V_{\alpha,\beta} = \alpha V(x) + \beta V(x - \frac{1}{2})$. This equation can be solved explicitly

$$f(x) = \frac{\exp(-\frac{2}{\sigma^2}[\alpha\phi(x) + \beta\phi(x - \frac{1}{2})])}{\int_I \exp(-\frac{2}{\sigma^2}[\alpha\phi(y) + \beta\phi(y - \frac{1}{2})])dy}$$

with $\phi(x) = \int_I V(z)dz$, so $\phi(x) = \phi(-x)$.

Assume $\phi(\frac{1}{2}) \neq 0$, which is generally the case. The condition for having two peaks concentrated at $x = 0$ and $x = \frac{1}{2}$ is that $\alpha\phi(x) + \beta\phi(x - \frac{1}{2})$ reaches its minimum at these points. In particular $\alpha\phi(0) + \beta\phi(-\frac{1}{2}) = \alpha\phi(\frac{1}{2}) + \beta\phi(0)$. This can only happen for $\alpha = \beta = \frac{1}{2}$.

What are the conditions on V for either one or two peaks of equal size to occur? Suppose for $\sigma << 1$ exists a peak-like smooth function f, mainly concentrated at 0, which solves

$$\frac{\sigma^2}{2}\partial_x f(x) + f(x) \int_I V(x-y) f(y) dy = 0 \ , \ \int_I f(x) dx = 1$$

and converges to δ_0 for $\sigma \to 0$. This function may be approximated by the solution of

$$\frac{\sigma^2}{2}\partial_x f(x) + f(x) V(x) = 0 \ , \ \int_I f(x) dx = 1 \ .$$

Therefore

$$f(x) = \frac{\exp(-\frac{2}{\sigma^2}[\int_0^x V(z)dz])}{\int_I \exp(-\frac{2}{\sigma^2}[\int_0^y V(z)dz])dy} \ .$$

For $\int_0^{\frac{1}{2}} V(x)dx > 0$ we have a main concentration around 0. For $\int_0^{\frac{1}{2}} V(x)dx < 0$ the peak is located at $\pm\frac{1}{2}$, which is a contradiction. Similar conditions for N-peaks like steady states can be obtained.

6. Stability/Instability of N-Peaks Like Steady States

This analysis was done by numerical simulations with a robust code

- Taking V such, that a 1-peak like steady state can be constructed, it follows, that the 2-peaks like steady state is unstable.
- Otherwise, the 2-peaks like steady state is stable.

- The 4-peaks like steady state seems unstable, independent of V.

References

[1] M. Dworkin and D. Kaiser (eds), *Myxobacteria II*, American Society for Microbiology Press (1993).

[2] E. Geigant, *Stability analysis of a peak solution of an orientational aggregation model*, EQUADIFF 99: Proceedings of the International Conference on Differential Equation, World Scientific, II (2000), 1210-1216.

[3] K. Kang, B. Perthame, A. Stevens and J.J.L. Velázquez, *An integro-differential equation model for alignment and orientational aggregation*, J. of Differential Equations **246**, no. 4 (2009), 1387–1421.

[4] I. Primi, A. Stevens and J.J.L. Velázquez, *Mass-Selection in Alignment Models with Non-Deterministic Effects*, Comm. Partial Differential Equations **34**, no. 4-6 (2009), 419–456.

Interfaces moving through random obstacles

Nicolas Dirr

(joint work with J. Côville, S. Luckhaus, P. Dondl, M. Scheutzow)

We consider the following so-called *Random Obstacle Model:* An interface, modelled as the graph $(x, u(x,t))$ of a function $u : \mathbb{R}^n \times \mathbb{R}^+ \to \mathbb{R}$ moves through a field of (soft) random obstacles, driven by a constant driving force. More precisely, we consider the following semi-linear PDE with random coefficients.

$$\partial_t u(x,t,\omega) = \Delta u(x,t,\omega) + f(x, u(x,t,\omega), \omega) + F \quad \text{on } \mathbb{R}^n \tag{1}$$

$$u(x,0) = 0 \tag{2}$$

The random nonlinearity $f(x,u,\omega) : \mathbb{R}^n \times \mathbb{R} \times \Omega \to \mathbb{R}$ is constructed in the follwing way: Let ϕ be the mollification of a cylindrical obstacle of height and radius $0 < \delta < 1/4$ centered at zero, i.e. Φ smooth and nonnegative,

$$1_{[-(3\delta)/4,(3\delta)/4]\times B_{(3\delta)/4}(0)}(x,u) \le \Phi(x,u) \le 1_{[-\delta,\delta]\times B_\delta(0)}(x,u).$$

$$f(x,u) = \sum\nolimits_{(i,j)\in\mathbb{Z}^n\times(\mathbb{Z}+\frac{1}{2})} \left(\mathbb{E}(\ell_{ij}) - \ell_{i,j}(\omega)\right) \phi(x-i, u-j).$$

Here the random obstacles $(\ell_{i,j}(\omega))_{(i,j)\in\mathbb{Z}^n\times(\mathbb{Z}+\frac{1}{2})}$ are a family of independent identically distributed exponential random variables. (i.e. there exists $\lambda_0 > 0$ such that $\mathbb{P}\{\ell(i,j)(\omega) > r\} = e^{-\lambda_0 r}$ for $r \ge 0$) and the constant $F > 0$ is the driving force. Typically $f(x,u,\omega) + F \le 0$ (interface pushed down) on the obstacles and $f(x,u,\omega) + F \ge 0$ (interface pushed up) away from the obstacles. Note that there are no obstacles on $\{(x,u) : \ |u| < 1/4\}$.

In the physics literature, a parabolic semi-linear equations with random coefficients like (1) is sometimes called Quenched Edwards Wilkinson model.

It is motivated in the following way: A very basic model for an interface (phase boundary, dislocation line in its slip plane etc) moving through an array of random obstacles (e.g. impurities, other dislocation lines) in an over-damped limit (inertial effects are neglected) is the gradient flow of the area functional plus a random bulk term. If so-called inner variations are considered, the resulting evolution

law is *forced mean curvature flow*, where the forcing is random. For forced mean curvature flow and applications, in particular in the case of periodic forcing, we refer to [1], [2], [3]. If the interface is a graph and the gradient is sufficiently small, the evolution by forced mean curvature flow for the graph can be approximated heuristically by a semi-linear parabolic PDE as (1).

Related problems have found considerable interest in the physics community, see e.g. [5].

The forcing F pushes the interface up, while the obstacles (which are not uniformly bounded) try to keep the interface down. Which effect wins? For *periodic* $f(x,u)$ this is completely understood (see [4]). We ask whether, depending on F, $\lim_{t\to\infty} u(x,t)$ is finite (pinning) or infinite (no pinning). (Note that there are by construction no obstacles on $\{u=0\}$ so it is easy to see that always $\partial_t u \geq 0$) By the comparison principle for (1), any global non-negative stationary solution acts as barrier for (1,2), so it it is sufficient to consider existence or non-existence of solutions for

$$\left\{ \begin{array}{rcl} 0 & = & \Delta u(x,\omega) + f(x,u(x,\omega),\omega) + F \quad \text{on } \mathbb{R}^n \\ u(x) & \geq & 0 \end{array} \right. . \tag{3}$$

Theorem 1 [N.D., J. Coville, S. Luckhaus] Let the space dimension $n=1$ and let u solve (3) on $[-N,N]$ with $u(-N)=u(N)=0$. Then there exist $F_0>0$, C and K such that for $F>F_0$

$$\mathbb{P}\Big(u(x) \geq KN - K|x| \text{ for all } x\in[-N,N]\Big) \geq 1 - Ce^{-\frac{N}{C}} \tag{4}$$

Corollary 1 $[n=1]$ There is almost surely no global non-negative stationary solution of (3).

Theorem 2 [N.D., P. Dondl, M. Scheutzow] Let $n=1,2$. There ex. $0<F_1$ such that for $0<F<F_1$, (3) has almost surely a solution with $\mathbb{E}[u(x,\omega)]=c<\infty$ for all $x\in\mathbb{R}^n$.

Sketch of Proof of Theorem 1

Using that stationary solutions solve $u_{xx}=-F$ away from the obstacles, we define a discretization yielding a discretized path $\bar{v}^\delta : \mathbb{Z}\to\delta\mathbb{Z}$. Then we estimate the discrete Laplacian of $\bar{v}^\delta(i)$ against the obstacle that sits above i and is close to the path, i.e. $\Delta_d(i)+F \leq C\ell_{i,[\bar{v}^\delta(i)[}(\omega)$. A technical problem is posed by the fact that a path with large gradients may pass through more than one of the obstacles sharing the same u-coordinate.

The estimate allows to bound the probability of a discrete path being "compatible" with the random environment against an auxiliary random *product* measure on discrete paths, i.e. independence is artificially introduced:

$$\begin{aligned} \mathbb{P}\left(\{\omega:\ u(\omega) \text{ compatible with } \bar{v}^\delta(i)\}\right) &\leq C^{2N}\hat{\mathbb{P}}\left(\{\Delta_d\bar{v}^\delta(i)\}_{i=-N}^N\right), \\ \hat{\mathbb{P}}\left(\{\Delta_d\bar{v}^\delta(i)\}_{i=-N}^N\right) &:= Z^{-1}e^{-C\sum_i\left(\Delta_d\bar{v}^\delta(i)+F\right)_+}, \end{aligned}$$

where Z is a normalization (corresponding to the partition function is statistical mechanics).

Notice that under the auxiliary measure, the discrete Laplacians are independent random variables with exponential tails. Paths that are in the complement of the set estimated in (4) have an average of discrete Laplacians which is different from the expectation under $\hat{\mathbb{P}}$. Such an event has exponentially small probability.

Sketch of Proof of Corollary 1

This follows from the Borel-Cantelli Lemma and the fact that, by the comparison principle for the parabolic equation (1), any global non-negative stationary solution has to remain above the solution of the Dirichlet problems considered in Theorem 1.

Sketch of Proof of Theorem 2 The aim is to contruct a stationary nonnegative supersolution.

We decompose $\mathbb{R}^n \times \mathbb{R}^+$ in large cubes of sidelength L and height h and call a cube *open* if it contains an obstacle with strength larger than an approriately chosen cut-off. We would like to construct a Lipschitz-path w with Lipschitz constant depending on h/L, which crosses only open cubes. Mapping the cubes to sites on the integer lattice, this corresponds to asking whether the percolating cluster of open sites contains a Lipschitz graph. We construct the graph explicitly by an iterative procedure and show, using properties of branching processes, that the iteration terminates, if open sites are sufficiently frequent. The latter property depends on the choice of the cut-off, h, L and the tail of the distribution of obstacle strengths.

From w we construct a function $v \geq 0$ with Lipschitz-constant $C(F, h/L)$ which solves $\Delta v = -F$ outside the strong obstacles and equals w on the boundary of strong obstacles. The choice of $C(F, h, L)$ allows to estimate the normal derivative on the boundary of the obstacles, which in turn allows to extend the construction of a supersolution inside the obstacles by paraboloids.

References

[1] P. Cardaliaguet, P.L. Lions and P. E. Souganidis, *A* discussion about the homogenization of moving interfaces, (English, French summary) J. Math. Pures Appl. **91** (2009), 339–363.

[2] B. Craciun and K. Bhattacharya,, *Effective motion of a curvature-sensitive interface through a heterogeneous medium*, Interfaces Free Bound., **6**, (2004), 151–173.

[3] N. Dirr, G. Karali, G. and N. K. Yip, *Pulsating wave for mean curvature flow in inhomogeneous medium*, **19**, (2008), 661–699.

[4] N. Dirr and N. K. Yip, *Pinning and de-pinning phenomena in front propagation in heterogeneous media*, Interfaces Free Bound., **8**, (2006), 79–109.

[5] W. Kleemann, *Dynamic phase transitions in ferroic systems with pinned domain wall.* In: Abstracts from the Workshop "Phasenübergänge" held June 20–26, 2004, Organized by H.W. Alt, S. Luckhaus, E. Presutti and E.K.H. Salje, Oberwolfach Reports **1** (2004), 1587–1656.

About a derivation of boundary layer energies by Γ-convergence methods

Anja Schlömerkemper
(joint work with Lucia Scardia, Chiara Zanini)

Let a crack occur in a solid body. Then new surface is created. Our aim is to rigorously derive the energy needed to create this surface. We call this energy boundary layer energy and study a one-dimensional model case which shows elastic behavior as well as fracture depending on the overall deformation of the system [2]. The starting point of the analysis is a chain of atoms with nearest and next-to-nearest neighbor interactions of Lennard-Jones type. We pass to the continuum limit by using Γ-convergence methods. While the Γ-limit yields the bulk energy, the first-order Γ-limit yields the boundary layer energies.
Our work extends an earlier article by Braides and Cicalese [1]. In addition to the Dirichlet boundary conditions which fix the positions of the first and last atoms we also prescribe the positions of the second and last but one atoms. This results in new Γ-limits of first order and in new results related to the location of cracks, which are outlined below.

For simplicity of this presentation let J_1 and J_2 be Lennard-Jones potentials, i.e., let $J_1(z)$ as well as $J_2(z)$ be of the form $\frac{k_1}{z^{12}} - \frac{k_2}{z^6}$ for positive constants k_1, k_2. See [2] for more general potentials. Set $\lambda_n = \frac{1}{n}$, $n \in \mathbb{N}$ and let $u : \lambda_n\mathbb{Z} \cap [0,1] \to \mathbb{R}$ describe the deformation of the atoms with respect to the reference configuration $\lambda_n\mathbb{Z} \cap [0,1]$. Set $u^i = u(\lambda_n i)$ and identify u with its piecewise affine interpolation, $u \in \mathcal{A}_n(0,1)$. Let ℓ, $u_0^{(1)}$, $u_1^{(1)} > 0$ be given. Then we consider the boundary conditions $u^0 = 0, u^1 = \lambda_n u_0^{(1)}, u^{n-1} = \ell - \lambda_n u_1^{(1)}, u^n = \ell$ and the energy functional $H_n^\ell : \mathcal{A}_n(0,1) \to (-\infty, \infty]$ which is defined as

$$H_n^\ell(u) = \sum_{i=0}^{n-1} \lambda_n J_1\left(\frac{u^{i+1} - u^i}{\lambda_n}\right) + \sum_{i=0}^{n-2} \lambda_n J_2\left(\frac{u^{i+2} - u^i}{2\lambda_n}\right)$$

if u satisfies the boundary conditions and is infinite else. The Γ-limit of this functional as $n \to \infty$ involves the convexification J_0^{**} of the effective potential

$$J_0(z) = J_2(z) + \frac{1}{2}\inf\big\{J_1(z_1) + J_1(z_2) : z_1 + z_2 = 2z\big\}.$$

Theorem 0.1. *Let J_1 and J_2 be Lennard-Jones potentials. Then the Γ-limit of H_n^ℓ with respect to the $L^1(0,1)$-topology exists and is given, on $L^1(0,1)$, by*

$$H^\ell(u) = \int_0^1 J_0^{**}(u'(t))\,dt$$

if $u \in BV(0,1)$ satisfies $u(0) = 0$, $u(1) = \ell$ and $[u] > 0$ on S_u, and infinity else.

The minimum of H^ℓ is $J_0^{**}(\ell)$. This enters in the calculation of the first-order Γ-limit. The first-order Γ-limit of H_n^ℓ is the Γ-limit of $H_{1,n}^\ell : \mathcal{A}_n(0,1) \to (-\infty, \infty]$ defined by $H_{1,n}^\ell(u) = \frac{1}{\lambda_n}\left(H_n^\ell(u) - \min H^\ell\right)$.

From the assumptions on the interaction potentials J_1 and J_2 it turns out that J_0 has a unique minimum point. This is denoted by γ and acts as a threshold for the overall deformation ℓ, determining whether we are in the case of elasticity ($\ell \leq \gamma$) or in the case of fracture ($\ell > \gamma$). In the case of elasticity we obtain

Theorem 0.2. *Let $0 < \ell \leq \gamma$ and $u_0^{(1)}, u_1^{(1)} > 0$; let J_1, J_2 be Lennard-Jones potentials. Then $H^\ell_{1,n}$ Γ-converges with respect to the $L^\infty(0,1)$-topology to H^ℓ_1 defined on $W^{1,\infty}(0,1)$ by*

$$H_1^\ell(u) = B\left(u_0^{(1)}, \ell\right) + B\left(u_1^{(1)}, \ell\right) - J_0(\ell) - J_0'(\ell)\left(\frac{u_0^{(1)} + u_1^{(1)}}{2} - \ell\right)$$

if $u(t) = \ell t$, $t \in [0,1]$ and infinity else, where, for $\theta > 0$,

$$\begin{aligned} B(\theta, \ell) = \inf_{N \in \mathbb{N}} \min \Bigg\{ & \frac{1}{2} J_1(\theta) + \sum_{i \geq 0} \Bigg\{ J_2\left(\frac{v^{i+2} - v^i}{2}\right) + \frac{1}{2} J_1\left(v^{i+2} - v^{i+1}\right) \\ & + \frac{1}{2} J_1\left(v^{i+1} - v^i\right) - J_0(\ell) - J_0'(\ell)\left(\frac{v^{i+2} - v^i}{2} - \ell\right) \Bigg\} : \\ & v : \mathbb{N} \to \mathbb{R}, v^0 = 0, v^1 = \theta, v^{i+1} - v^i = \ell \text{ if } i \geq N \Bigg\} \end{aligned}$$

is the boundary layer energy which occurs at the end points of $[0,1]$.

The case of fracture involves the formation of new surface, which translates in the presence of some boundary layer energies. If the fracture is located at the boundary, this involves, for $\theta > 0$, a boundary layer energy of the form

$$\begin{aligned} B_b(\theta) = \inf_{k \in \mathbb{N}} \min \Bigg\{ & \frac{1}{2} J_1\left(\widehat{v}^1 - \widehat{v}^0\right) + \sum_{i=0}^{k-1} \Bigg\{ J_2\left(\frac{\widehat{v}^{i+2} - \widehat{v}^i}{2}\right) \\ & + \frac{1}{2}\left(J_1\left(\widehat{v}^{i+2} - \widehat{v}^{i+1}\right) + J_1\left(\widehat{v}^{i+1} - \widehat{v}^i\right)\right) - J_0(\gamma) \Bigg\} : \\ & \widehat{v} : \mathbb{N} \to \mathbb{R}, \widehat{v}^{k+1} = 0, \widehat{v}^{k+1} - \widehat{v}^k = -\widehat{v}^k = \theta \Bigg\}. \end{aligned}$$

This boundary layer energy reflects the position of the crack at the atomistic scale. The boundary layer energy of a free surface was introduced in [1], and reads

$$\begin{aligned} B(\gamma) = \inf_{N \in \mathbb{N}} \min \Bigg\{ & \frac{1}{2} J_1\left(u^1 - u^0\right) + \sum_{i \geq 0} \Bigg\{ J_2\left(\frac{u^{i+2} - u^i}{2}\right) \\ & + \frac{1}{2}\left(J_1\left(u^{i+2} - u^{i+1}\right) + J_1\left(u^{i+1} - u^i\right)\right) - J_0(\gamma) \Bigg\} : \\ & u : \mathbb{N} \to \mathbb{R}, u^0 = 0, u^{i+1} - u^i = \gamma \text{ if } i \geq N \Bigg\}. \end{aligned}$$

In the case of fracture the first-order Γ-limit is as follows.

Theorem 0.3. *Let $\ell > \gamma$ and $u_0^{(1)}$, $u_1^{(1)} > 0$; let J_1, J_2 be Lennard-Jones potentials. Then $H_{1,n}^{\ell}$ Γ-converges with respect to the $L^1(0,1)$-topology to H_1^{ℓ} defined on $L^1(0,1)$ by*

$$\begin{aligned} H_1^{\ell}(u) =& B\left(u_0^{(1)}, \gamma\right)(1 - \#(S_u \cap \{0\})) + B\left(u_1^{(1)}, \gamma\right)(1 - \#(S_u \cap \{1\})) \\ &+ B_{BJ}\left(u_0^{(1)}\right)\#(S_u \cap \{0\}) + B_{BJ}\left(u_1^{(1)}\right)\#(S_u \cap \{1\}) \\ &+ B_{IJ}\#(S_u \cap]0,1[) - J_0(\gamma) \end{aligned}$$

if $u \in SBV(0,1)$ such that $u(0-) = 0$, $u(1+) = \ell$, $0 < \#S_u < \infty$, $[u] > 0$ on S_u and $u' = \gamma$ a.e., and infinity else, where

$$\begin{aligned} B_{BJ}(\theta) &= \frac{1}{2}J_1(\theta) + B_b(\theta) + B(\gamma) - 2J_0(\gamma) \\ B_{IJ} &= 2B(\gamma) - 2J_0(\gamma). \end{aligned}$$

While, in the model considered in [1], the energetically favourable location of a crack is at the boundary of the chain, our model shows that the optimal deformation can exhibit an internal crack.

Proposition 0.4. *Let $\ell > \gamma$ and J_1, J_2 be Lennard-Jones potentials.*

(1) *If $u_0^{(1)} = u_1^{(1)} = \gamma$, then it is energetically as favorable to break in the interior as at the boundary of the chain.*
(2) *If $u_0^{(1)}$ or $u_1^{(1)}$ is equal to δ_1, the minimum point of J_1, then the chain breaks at the boundary.*

By studying the infimum in the definitions of the boundary layer energies, we obtain information on the "depth" of the boundary layer. For instance, in the case of a crack in 0 with $u_0^{(1)} = \delta_1$ we prove that the microscopic location of the crack is just next to the prescribed boundary atoms since the infimum in $B_b(\delta_1)$ is attained for $k = 0$. Similarly, if $u_0^{(1)} = \gamma$, the infimum in the elastic boundary layer energy $B(\gamma, \gamma)$ at 0 is attained for $N = 0$, meaning that prescribing the slope γ at the boundary forces the optimal deformation to have slope γ close to the boundary also at the atomic scale. On the other hand, the infimum in $B(\gamma)$ is obtained for $N \to \infty$. Therefore in the case of a free surface, the discrete system adjusts to the optimal slope γ after infinitely many atoms. Similarly, the infimum in $B_b(\gamma)$ is obtained for $k \to \infty$. That is, even if there is a crack at 0 in the continuum framework, microscopically, the crack occurs after infinitely many atoms.

References

[1] A. Braides and M. Cicalese, *Surface energies in nonconvex discrete systems*, Math. Models Methods Appl. Sci. **17** (2007), 985–1037

[2] L. Scardia, A. Schlömerkemper, C. Zanini, *Boundary layer energies for nonconvex discrete systems*, submitted, MPI-MIS preprint 4/2009

A quantitative rigidity result for the cubic-to-tetragonal phase transition in the geometrically linear theory with interfacial energy

Felix Otto
(joint work with Antonio Capella-Kort)

In *geometrically linear* elasticity, the strain e generated by a displacement u is approximated by $e = \frac{1}{2}(\nabla u + \nabla^t u)$. In the cubic-to-tetragonal phase transition in a shape memory alloy, there are three different *stress-free* strains (which we normalize)

$$e^{(1)} := \begin{pmatrix} -2 & 0 & 0 \\ 0 & 1 & 0 \\ 0 & 0 & 1 \end{pmatrix}, \quad e^{(2)} := \begin{pmatrix} 1 & 0 & 0 \\ 0 & -2 & 0 \\ 0 & 0 & 1 \end{pmatrix}, \quad e^{(3)} := \begin{pmatrix} 1 & 0 & 0 \\ 0 & 1 & 0 \\ 0 & 0 & -2 \end{pmatrix}.$$

In this framework, Dolzmann and Müller [2, Theorem 3.1] have shown the following *rigidity* result: The only stress-free configurations are (locally) *twins*. A twin is a configuration where e only depends on a *single* variable and only assumes *two* values. In a cubic-to-tetragonal phase transition, there are *six* types of twins: If e assumes the values $e^{(1)}$ and $e^{(2)}$, say, then e must be either locally constant along the planes $x_1 + x_2 = const$ or along the planes $x_1 - x_2 = const$. The two other cases are similar by cubic symmetry.

It is well-known that rigidity results of this type are vulnerable under perturbation: Indeed, consider a piecewise quadratic elastic energy (with normalized moduli), which can be written as

$$E_{elast} := \int_{B_1} |e - \chi_1 e^{(1)} - \chi_2 e^{(2)} - \chi_3 e^{(3)}|^2 dx,$$

where

$$\chi_1,\ \chi_2,\ \chi_3 \ \in \{0,1\} \quad \text{and} \quad \chi_0 := 1 - \chi_1 - \chi_2 - \chi_3 \in \{0,1\},$$

so that the characteristic functions χ_0, χ_1, χ_2, and χ_3 can be interpreted as the indicator functions of the Austenite phase (which here is assumed to be also stress-free) and the three Martensitic phases, respectively. The best-studied rigidity result is related to a mixture of Austenite and Martensite: There is no displacement u with a stress-free strain e assuming the value zero *and* at least one of the three values $e^{(1)}$, $e^{(2)}$, and $e^{(3)}$. In particular, there is no exactly stress-free interface between a Martensitic twin (with twin plane $x_1 + x_2 = const$, say) on the one side and Austenite on the other side. However, the elastic energy of such a configuration can be made arbitrarily small by forming a *microstructure*, i. e. 1) by letting the twin width ℓ tend to zero, and 2) by choosing the twin volume fraction λ (i. e. the relative width of one layer w. r. t. the other layer) appropriately (i. e. $\lambda = \frac{1}{3}$ or $\lambda = \frac{2}{3}$), and 3) by choosing the habit plane (i. e. the plane between the Martensitic twin and the Austenite) appropriately (i. e. $x_1 + x_3 = const$, $x_1 - x_3 = const$, $x_2 + x_3 = const$, or $x_2 - x_3 = const$).

This degeneracy of the elastic energy can be compensated by an interfacial energy between the phases:

$$E_{interf} := \int_{B_1} (|\nabla\chi_0| + |\nabla\chi_1| + |\nabla\chi_2| + |\nabla\chi_3|)dx,$$

whose role is to penalize the microstructure. The introduction of an interfacial energy next to the elastic energy introduces a (material) length scale; together with the length scale given by the sample size (unity in our case), it gives rise to a nondimensional parameter $\eta \ll 1$. Theorem 1 below shows that the *scaling* of $\eta^{1/3}E_{interf} + \eta^{-2/3}E_{elast}$ *discriminates* between configurations that are close to configurations with *exactly* vanishing elastic energy (that is, pure Austenite or one of the six Martensitic twins) and the other configurations. In this sense, we may say that the interfacial energy *unfolds* the degenerate elastic energy.

The pair of exponents $\frac{2}{3}$, $1 - \frac{2}{3} = \frac{1}{3}$ in $\eta^{1/3}E_{interf} + \eta^{-2/3}E_{elast}$ already appeared in Kohn and Müller's study of the interface between a twinned Martensite and an Austenite phase on the level of a simplified, in particular scalar and two-dimensional model [3, 4]. Naively, one would expect that the minimal energy is found by optimizing the twin width ℓ, which would lead to the pair of exponents $\frac{1}{2}, 1 - \frac{1}{2} = \frac{1}{2}$. This however is *not* the optimal energy scaling: A small twin width ℓ is only required near the Austenite-Martensite interface. Hence it is advantageous to refine ℓ by twin *branching* when approaching this interface. Such a branched construction indeed leads to the better pair of exponents $\frac{1}{3}, 1 - \frac{1}{3} = \frac{2}{2}$. By proving an *Ansatz-free lower bound* [4, Theorem 1.1], Kohn and Müller show that this pair of exponents cannot be improved.

Hence Theorem 1 combines the qualitative treatment (rigidity) of the full model in [2] with the quantitative treatment (Ansatz-free lower bounds optimal in scaling) of the reduced model in [4]. It improves our result in [1] in the sense that Theorem 1 includes the Austenite phase and that it is a local statement.

Theorem 1. *There exists a small but universal radius $r > 0$ and a universal constant C such that we have for any parameter $\eta \leq r$: If χ_0, χ_1, χ_2, χ_3, e, E_{interf} and E_{elast} are as above and we use the abbreviation*

$$E := \eta^{1/3}E_{interf} + \eta^{-2/3}E_{elast},$$

then the following three dichotomies hold:

i) *We have*

$$\int_{B_r} |1 - \chi_0|dx \leq C\,E \quad \underline{or} \quad \int_{B_r} |\chi_0|dx \leq C\,E.$$

ii) *In case of $\int_{B_r} |\chi_0|dx \leq C\,E$, we have*

$$\int_{B_r} |\chi_1|dx \leq C\,E^{1/2} \ \underline{or} \ \int_{B_r} |\chi_2|dx \leq C\,E^{1/2} \ \underline{or} \ \int_{B_r} |\chi_3|dx \leq C\,E^{1/2}.$$

iii) *In case of* $\int_{B_r} |\chi_3| dx \leq C\, E^{1/2}$, *we have*

$$\int_{B_r} |\chi_1 - f_{(110)}| dx \leq C\, E^{1/4} \quad \underline{or} \quad \int_{B_r} |\chi_1 - f_{(1\bar{1}0)}| dx \leq C\, E^{1/4},$$

where $f_{(110)}$, $f_{(1\bar{1}0)}$ *denote functions only depending on* $x \cdot (110) = x_1 + x_2$ *and* $x \cdot (1\bar{1}0) = x_1 - x_2$, *respectively. In the two other cases, the analogue statement holds.*

References

[1] A. Capella-Kort, F. Otto, A rigidity result for a perturbation of the geometrically linear three-well problem, *Comm. Pure Applied Math.* **62 (12)** (2009)

[2] G. Dolzmann, S. Müller, The influence of surface energy on stress-free microstructures in Shape Memory Alloys, *Meccanica* **30**, 527-539 (1995)

[3] R. V. Kohn, S. Müller, Branching of twins near an austenite-twinned-martensite interface, *Philosophical Magazine A* **66 (5)**, 697-715 (1992)

[4] R. V. Kohn, S. Müller, Surface energy and microstructure in coherent phase transitions, *Comm. Pure Applied Math.* **47**, 405-435 (1994)

Evolution in dilute diblock-copolymer systems

Barbara Niethammer

(joint work with M. Helmers, Y. Oshita, X. Ren)

Diblock copolymers molecules consist of two subchains of A- and B-monomers, which repel each other below a critical temperature. However, due to a chemical bond between the subchains, complete phase-separation between A- and B-monomers can not take place. Instead molecules rearrange themselves to form domains rich of A- and B-monomers respectively, a phenomenon known as micro phase separation.

In a sharp interface version of the Ohta-Kawasaki theory energetically favorable configurations are characterized as minimizers of an energy functional that is defined on subsets $G \subset \Omega \subset \mathbb{R}^3$ with given volume fraction ρ, that represent the domains covered by, say, A-monomers. Then

$$E(G) = \mathbf{H}^2(\partial G) + \frac{\sigma}{2} \|\chi_G - \rho\|^2_{H^{-1}(\Omega)},,$$

with a material parameter σ. The first term in the energy, the surface area of ∂G, favors phase separation, whereas the second one prefers fine structures and the competition between the two terms leads to pattern formation. The type of pattern that is observed is essentially determined by the volume fraction ρ and ranges from droplet patterns, over cylindrical structures to layers.

In this talk we are interested in a dynamic model that describes the evolution of systems towards their equilibrium configuration. One way to set up such an evolutionary model is to consider the H^{-1} gradient flow of $E(G)$ on the manifold of domains G with given volume fraction. This leads to a nonlocal version of the so-called Mullins-Sekerka free boundary problem.

Here we consider the regime that the volume fraction of A-monomers is small. Then micro phase separation results in an ensemble of small spheres of one component. It is then natural to study the gradient flow evolution restricted to the submanifold that consists of a collection of non-overlapping balls. We consider the setting that balls of radius R with average spacing d are set in a box of length L. An important intrinsic length scale is given by the screening length $L_{sc} \sim (d^3/R)^{1/2}$, that describes the effective interaction range between particles. In the regime that $\rho \ll 1$ we can then set up the gradient flow equation for the evolution of radii and centers of these balls. By superposition of monopoles we can express energy and metric explicitly in terms of the radii and centers of the balls and form this derive explicit expressions for the velocities of radii and centers respectively [2] (see also [1] for a related result). The regime $L \ll L_{sc}$ is particularly simple: the energy depends to leading order not on the positions of the centers and the metric tensor is to leading order diagonal. Then, particle centers do not move in this regime, whereas the radii obey a relatively simple nonlocal ODE. This ODE predicts that the balls first undergo coarsening, before settling around one stable radius. The regime $L \sim L_{sc}$ is more interesting in the sense, that one also obtains a non-trivial equation for the centre velocities. However, the centers move on a slower time scale than the radii. Hence, we observe first coarsening of radii, then stabilization of radii around one radius, and then rearrangement of particle centers. One observes in numerical simulations that the latter results in a periodic pattern of the balls, but a rigorous analysis of this effect is not yet available.

One can also derive corresponding mean-field models that describe the evolution of a density of particle radii and centers. I indicate how this can be made rigorous by passing to a homogenization limit within the Rayleigh principle associated to each gradient flow [3]. This generalizes a result obtained in [4] for $\sigma = 0$ to the case $\sigma > 0$. The main new ingredient is an a-priori estimate on the velocities of particle centers, that ensures that if particles are initially well-separated then they remain well-separated during the evolution over the time scales we consider.

References

[1] K. Glasner and R. Choksi. Coarsening and Self-organization in Dilute Diblock Copolymer Melts and Mixtures, *Physica D*, **238**, 1241–1255 (2009).

[2] M. Helmers, B. Niethammer and X. Ren. Evolution in off-critical diblock-copolymer melts. *Networks Heterogeneous Media*, **3-3**, 615–632, (2008).

[3] B. Niethammer and Y. Oshita. A rigorous derivation of mean-field models for diblock copolymer melts, Preprint (2009).

[4] B. Niethammer and F. Otto. Ostwald Ripening: The screening length revisited. *Calc. Var. and PDE*, **13-1**, 33–68, (2001).

On single-slip plasticity in the limit of rigid elasticity

Sergio Conti
(joint work with Georg Dolzmann, Carolin Klust, Stefan Müller)

Variational models which combine energetic and dissipative terms are often used in finite plasticity to study the formation of microstructure under monotonic loading conditions [12, 9, 2]. The simplest model, proposed and first studied in [12], treats one active slip system with rigid elasticity, in the sense that the only admissible elastic deformations of the material are (locally) rigid body motions. It consists in the minimization of $\int_\Omega W_{\rm R}(\nabla u)$, where the condensed energy density takes the form

$$W_{\rm R}(F) = \begin{cases} |\gamma|^p & \text{if } F = Q(\mathrm{Id} + \gamma s \otimes m)\,, \\ \infty & \text{otherwise}\,. \end{cases} \tag{1}$$

Here $p \geq 1$ and s, m are a pair of orthonormal vectors describing the slip direction and the slip-plane normal. Based on this model, the formation of microstructure (with $p = 1$) was predicted, and the phenomenon of geometrical softening [12] was explained. Related models were discussed in [2, 8, 1]. The quasiconvex envelope of the rigid model $W_{\rm R}$ could be determined in closed form for several values of the hardening exponent p:

Theorem 1 (From [7, 3, 4]). *For $n = 2$, $p = 1$, the quasiconvex envelope of $W_{\rm R}$ is given by*

$$W_{\rm R}^{\rm qc}(F) = \begin{cases} \sqrt{|F|^2 - 2\det F}\,, & \text{if } F \in \mathcal{N}\,, \\ \infty\,, & \text{otherwise}\,, \end{cases} \tag{2}$$

where

$$\mathcal{N} = \big\{F\colon\ \det F = 1,\ |Fs| \leq 1\big\}\,. \tag{3}$$

If $n = 2$ and $p \geq 2$, then

$$W_{\rm R}^{\rm qc}(F) = \begin{cases} \big(|Fm|^2 - 1\big)^{p/2}\,, & \text{if } F \in \mathcal{N}\,, \\ \infty\,, & \text{otherwise}\,, \end{cases}$$

with $\mathcal{N}$ defined in (3).
If $n = 3$, then $W_{\rm R}$ is quasiconvex.

We address here the approximation of $W_{\rm R}$ by a sequence of energy densities with increasingly hard elasticity, in the two-dimensional case. Precisely, we consider

$$W_\varepsilon(F) = \inf_{\gamma\in\mathbb{R}} \Big\{ \frac{1}{\varepsilon}\, \mathrm{dist}^2\big(F(\mathrm{Id} - \gamma s \otimes m), \mathrm{SO}(2)\big) + |\gamma|^p \Big\}\,.$$

It is easy to show that W_ε converges for $\varepsilon \to 0$ to W pointwise. This convergence, however, is not directly related to convergence of the corresponding functionals.

If the exponent p is below 2, then the variational problem degenerates:

Theorem 2 (From [5]). *For all $p \in [1, 2)$, one has $W_\varepsilon^{\rm qc}(F) = 0$ for all $F \in \mathcal{N}$.*

This is in remarkable contrast with the relaxation of the limiting energy for $p = 1$ given in (2).

A different picture arises for $p = 2$. Indeed, we obtain convergence of the variational problems $I_\varepsilon[u] = \int_\Omega W_\varepsilon(\nabla u)$ to the limit

$$I_0[u] = \begin{cases} \displaystyle\int_\Omega W_{\mathrm{R}}^{\mathrm{qc}}(\nabla u)dx\,, & \text{if } u \in W^{1,2}(\Omega;\mathbb{R}^2),\ \nabla u \in \mathcal{N} \text{ a.e. in } \Omega\,, \\ \infty\,, & \text{otherwise.} \end{cases}$$

The limiting problem is defined on a subset of $W^{1,2}$, but the appropriate convergence is weak $W^{1,1}$ convergence (after subtracting translations). This is related to the anisotropic growth of the potentials W_ε.

Theorem 3 (From [4]). *Let $\Omega \subset \mathbb{R}^2$ be a bounded and open Lipschitz domain, $p = q = 2$. Then the functionals $I_\varepsilon[u] = \int_\Omega W_\varepsilon(\nabla u)$ converge in the sense of Γ–convergence with respect to weak convergence in $W^{1,1}$ to I_0. That is, the following assertions hold true:*

Compactness and lower bound: *Suppose that $u_\varepsilon \in W^{1,1}(\Omega;\mathbb{R}^2)$ is a sequence with bounded energy, in the sense that there is $B < \infty$ such that $I_\varepsilon[u_\varepsilon] < B$ for all $\varepsilon > 0$. Then there exists a subsequence $\varepsilon_k \to 0$, a sequence $a_k \in \mathbb{R}^2$, and a function $u \in W^{1,2}(\Omega;\mathbb{R}^2)$ with $\nabla u \in \mathcal{N}$ almost everywhere such that $u_{\varepsilon_k} - a_k \rightharpoonup u$ weakly in $W^{1,1}(\Omega;\mathbb{R}^2)$. Moreover,*

$$I_0[u] = \int_\Omega W_{\mathrm{R}}^{\mathrm{qc}}(\nabla u) \le \liminf_{k\to\infty} \int_\Omega W_{\varepsilon_k}(\nabla u_{\varepsilon_k}) = \liminf_{k\to\infty} I_{\varepsilon_k}[u_{\varepsilon_k}]\,.$$

Upper bound: *For all $u \in W^{1,2}(\Omega;\mathbb{R}^2)$ with $\nabla u \in \mathcal{N}$ almost everywhere and all sequences $\varepsilon_k \to 0$, $\varepsilon_k > 0$, there exists a sequence of functions $u_{\varepsilon_k} \in W^{1,1}(\Omega;\mathbb{R}^2)$ with $u_{\varepsilon_k} \to u$ in $L^1(\Omega;\mathbb{R}^2)$ such that*

$$\lim_{k\to\infty} I_{\varepsilon_k}[u_{\varepsilon_k}] = I_0[u]\,.$$

One key difficulty in the proof resides in the anisotropic growth conditions of W_ε. In particular, the sequence of gradients ∇u_ε is bounded in L^1 but not in L^2, although the limit ∇u belongs to L^2. In order to show that $\det \nabla u_\varepsilon$ converges to $\det \nabla u$, and hence that the latter equals one, we use the following generalization of the classical div-curl lemma [10, 11, 13, 14]

Theorem 4 (From [6]). *Let $\Omega \subset \mathbb{R}^n$ be an open and bounded domain with Lipschitz boundary and let $p, q \in (1,\infty)$ with $1/p + 1/q = 1$. Suppose $u_k \in L^p(\Omega;\mathbb{R}^n)$, $v_k \in L^q(\Omega;\mathbb{R}^n)$ are sequences such that*

$$u_k \rightharpoonup u \quad \text{weakly in } L^p(\Omega;\mathbb{R}^n) \quad \text{and} \quad v_k \rightharpoonup v \quad \text{weakly in } L^q(\Omega;\mathbb{R}^n)\,,$$

and

$$u_k \cdot v_k \text{ is equi-integrable.}$$

Finally assume that

$$\operatorname{div} u_k \to \operatorname{div} u \quad \text{in } W^{-1,1}(\Omega) \quad \text{and} \quad \operatorname{curl} v_k \to \operatorname{curl} v \quad \text{in } W^{-1,1}(\Omega;\mathbb{R}^{n\times n})\,.$$

Then

$$u_k \cdot v_k \rightharpoonup u \cdot v \qquad \text{weakly in } L^1(\Omega)\,.$$

References

[1] Carstensen, C., Conti, S., and Orlando, A. Mixed analytical-numerical relaxation in finite single-slip crystal plasticity. *Cont. Mech. Thermod. 20* (2008), 275–301.

[2] Carstensen, C., Hackl, K., and Mielke, A. Non-convex potentials and microstructures in finite-strain plasticity. *R. Soc. Lond. Proc. Ser. A Math. Phys. Eng. Sci. 458*, 2018 (2002), 299–317.

[3] Conti, S. Relaxation of single-slip single-crystal plasticity with linear hardening. In *Multiscale Materials Modeling* (Freiburg, 2006), P. Gumbsch, Ed., Fraunhofer IRB, pp. 30–35.

[4] Conti, S., Dolzmann, G., and Klust, C. Asymptotic behavior of crystal plasticity with one slip system in the limit of rigid elasticity. *preprint* (2009).

[5] Conti, S., Dolzmann, G., and Klust, C. Relaxation of a class of variational models in crystal plasticity. *Proc. Roy. Soc. London A 465* (2009), 1735–1742.

[6] Conti, S., Dolzmann, G., and Müller, S. The div–curl lemma for sequences whose divergence and curl are compact in $W^{-1,1}$. *preprint* (2009).

[7] Conti, S., and Theil, F. Single-slip elastoplastic microstructures. *Arch. Ration. Mech. Anal. 178*, 1 (2005), 125–148.

[8] Miehe, C., Lambrecht, M., and Gürses, E. Analysis of material instabilities in inelastic solids by incremental energy minimization and relaxation methods: evolving deformation microstructures in finite plasticity. *J. Mech. Phys. Solids 52* (2004), 2725–2769.

[9] Miehe, C., Schotte, J., and Lambrecht, M. Homogeneization of inelastic solid materials at finite strains based on incremental minimiza tion principles. application to the texture analysis of polycrystals. *J. Mech. Phys. Solids 50* (2002), 2123–2167.

[10] Murat, F. Compacité par compensation. *Ann. Sc. Norm. Super. Pisa, Cl. Sci., IV. Ser. 5* (1978), 489–507.

[11] Murat, F. Compacité par compensation: condition necessaire et suffisante de continuite faible sous une hypothèse de rang constant. *Ann. Sc. Norm. Super. Pisa, Cl. Sci., IV. Ser. 8* (1981), 69–102.

[12] Ortiz, M., and Repetto, E. A. Nonconvex energy minimization and dislocation structures in ductile single crystals. *J. Mech. Phys. Solids 47*, 2 (1999), 397–462.

[13] Tartar, L. Une nouvelle méthode de résolution d'équations aux dérivées partielles non linéaires. Journ. d'Anal. non lin., Proc., Besancon 1977, Lect. Notes Math. 665, 228-241, 1978.

[14] Tartar, L. Compensated compactness and applications to partial differential equations. Nonlinear analysis and mechanics: Heriot-Watt Symp., Vol. 4, Edinburgh 1979, Res. Notes Math. 39, 136-212, 1979.

Uniform energy distribution for a model of pattern formation

Giovanni Alberti

(joint work with Rustum Choksi and Felix Otto)

In [1] we studied the qualitative behaviour of minimizers of the energy

$$I(u) := S(u) + \left\|(-\Delta)^{-1/2}(u-m)\right\|_2^2\,, \tag{1}$$

where m is a parameter in $(-1,1)$, u is a function on a "large" n-dimensional domain – typically the cube $Q_L := (-L/2, L/2)^n$ – taking only the values ± 1 and with average m, $S(u)$ is the area of the interface separating the phases $\{u = +1\}$

and $\{u = -1\}$, and $(-\Delta)^{-1}$ is the inverse of the Laplace operator with, say, Neumann boundary conditions. (In the end it turns out that boundary conditions do not really matter in this problem.)

More precisely, u belongs to the space $BV(Q_L, \pm 1)$ and $S(u)$ is the $(n-1)$-dimensional Hausdorff measure of the (measure theoretic) discontinuity set of u, or, equivalently,

$$S(u) = \frac{1}{2} \int_{Q_L} |Du|$$

where Du is the distributional derivative of u. Moreover the second term in the right-hand side of (1) is given by the (non-local) double integral

$$\iint_{Q_L \times Q_L} G(x, x') \, (u(x) - m) \, (u(x') - m) \, dx \, dx' \, ,$$

where G is the Green function associated to $(-\Delta)^{-1}$.

The energy in (1) can be obtained as the sharp-interface limit of the free-energy derived in [3] within a model of phase segregation for di-block copolymer melts; however its one-dimensional equivalent already attracted some attention in the mathematical community after [2] (for more details see [1] and the references therein).

While the first term at the right-hand side of (1) favours small interfaces, and therefore large phases, the second one favours fine phase-mixing with average density close to m (the latter effect can be easily seen in dimension one: in that case the second term can be written as $\int b^2$ where b is the antiderivative of $u - m$ with value 0 at the boundary).

As a result of the competition of these two terms, minimizers of $I(u)$ exhibit a fairly regular pattern on a fixed scale which is independent of the size of the domain L. In particular, numerical computations in dimension two and three display a variety of (essentially) periodic patterns, whose geometric shape and period depend only on the choice of the parameter m, and not on L.

In terms of rigorous results, the periodicity of minimizers in dimension one was established long time ago in [2] directly for the diffuse-interface counterpart of $I(u)$. Obtaining similar results in higher dimension proved to be more difficult; in [1] we aimed in that direction by proving the uniform distribution of energy for minimizers of $I(u)$ in every dimension.

In order to state our result we must formulate the problem in a different and more local way. The key observation is that the non-local term in $I(u)$ can be rewritten as

$$\inf \int_{Q_L} |b|^2 \, ,$$

where the infimum is taken over all vectorfields b which satisfy

$$\nabla \cdot b = u - m \text{ on } Q_L \text{ and } \nu \cdot b = 0 \text{ on } \partial Q_L. \tag{2}$$

Accordingly, the minimization of the non-local energy $I(u)$ turns into the minimization of the local energy

$$E(u,b,Q_L) := S(u) + \int_{Q_L} |b|^2 \tag{3}$$

over all couples (u,b) such that u takes the values ± 1 and has average m in Q_L, and b satisfies (2).

Our main result reads as follows: if (u_0,b_0) solves this minimum problem, then the average energy density in every subcube $Q_\ell(a)$ with center a and side ℓ gets closer and closer to an optimal density σ_* as ℓ gets larger. More precisely there exist constants c_1, c_2 – independent of L, u_0 and b_0 – such that

$$\left| \frac{1}{\ell^n} E(u_0,b_0,Q_\ell(a)) - \sigma_* \right| \le \frac{c_1}{\ell} \quad \text{for } \ell \ge c_2, \tag{4}$$

where the energy density σ_* is given by

$$\sigma_* := \lim_{L\to+\infty} \left\{ \inf_{(u,b)} \frac{1}{L^n} E(u,b,Q_L) \right\}$$

(clearly the infimum is taken over all (u,b) satisfying the conditions above).

I conclude with some remarks. (i) Note that σ_* should be the energy density of the ground state (optimal pattern), except that it is defined without assuming the existence of a ground state. Using (4) we can easily show that there exists a couple (u_*,b_*) defined on the entire space $\mathbf{R}^d$ which minimize the energy E with respect to every perturbation with compact support and satisfies $E(u_*,b_*,Q_L)/L^n \to \sigma_*$ as $L \to +\infty$. But we are not able prove that this "ground state" is periodic.

(ii) The decay rate in (4) cannot be improved even assuming the existence of a periodic ground state, and yet it is not such a strong indication of periodicity by itself, in that it is not sufficient to exclude truly non-periodic behaviours of (u_0,b_0), such as random checkerboard patterns.

(iii) A slightly stronger indication of periodicity can be obtained by looking at the deviation of the average of u_0 on large balls from the expected value m: denoting by $B_r(a)$ any ball of radius r contained in Q_L, we can prove that

$$\left| \frac{1}{|B_r(a)|} \int_{B_r(a)} u_0 - m \right| = O\left(\frac{1}{r^2}\right) \quad \text{as } r \to \infty,$$

and indeed this decay rate is better than that of a random checkerboard pattern, at least in dimensions two and three. On the other hand periodicity would imply a decay rate of order $o(1/r^p)$ for every $p < +\infty$, and therefore there is still a substantial gap.

References

[1] G. Alberti, R. Choksi, F. Otto, *Uniform energy distribution for an isoperimetric problem with long-range interactions*, J. Amer. Math. Soc. **22** (2009), 569–605.

[2] S. Müller, *Singular perturbations as a selection criterion for periodic minimizing sequences*, Calc. Var. Partial Differential Equations **1** (1993), 169–204.

[3] T. Ohta, K. Kawasaki, *Equilibrium morphology of block copolymer melts*, Macromolecules **19** (1986), 2621–2632.

Reporter: Barbara Zwicknagl

Participants

Prof. Giovanni Alberti
Dip. di Matematica "L.Tonelli"
Universita di Pisa
Largo Bruno Pontecorvo, 5
I-56127 Pisa

Yuen Au Yeung
Zentrum Mathematik
TU München
Boltzmannstr. 3
85748 Garching bei München

Dr. Basile Audoly
Institut Jean le Rond d'Alembert
Universite Pierre & Marie Curie
Paris VI, Case 162
4, place Jussieu
F-75252 Paris CEDEX 05

Prof. John M. Ball
Mathematical Institute
Oxford University
24-29 St. Giles
GB-Oxford OX1 3LB

Dr. Thomas Blesgen
Max-Planck-Institut für Mathematik
in den Naturwissenschaften
Inselstr. 22 - 26
04103 Leipzig

Prof. Dr. Sergio Conti
Institut für Angewandte Mathematik
Universität Bonn
Endenicher Allee 60
53115 Bonn

Prof. Dr. Kaushik Dayal
Carnegie Mellon University
Department of Civil and
Environmental Engineering
Pittsburgh PA 15213-3890
USA

Prof. Dr. Antonio DeSimone
SISSA
International School for Advanced
Studies
Via Beirut n. 2-4
I-34014 Trieste

Dr. Nicolas Dirr
Department of Mathematical Sciences
University of Bath
Claverton Down
GB-Bath BA2 7AY

Prof. Dr. Georg Dolzmann
Fakultät für Mathematik
Universität Regensburg
Universitätsstr. 31
93053 Regensburg

Prof. Dr. Ralf Drautz
ICAMS
Ruhr-Universität Bochum
Stiepeler Str. 129
44801 Bochum

Prof. Dr. Gilles Francfort
L.P.M.T.M.
Institut Galilee
Universite de Paris Nord
Ave. J. B. Clement
F-93430 Villetaneuse

Prof. Dr. Carlos J. Garcia-Cervera
Department of Mathematics
University of California at
Santa Barbara
South Hall
Santa Barbara , CA 93106
USA

Prof. Dr. Yury Grabovsky
Department of Mathematics
Temple University
Philadelphia , PA 19122
USA

Prof. Dr. Klaus Hackl
Lehrstuhl für Allgemeine Mechanik
Ruhr-Universität Bochum
Fakultät für Bauingenieurwesen
Universitätsstr. 150
44801 Bochum

Duvan Alberto Henao Manrique
Laboratoire Jacques-Louis Lions
Universite Pierre et Marie Curie
175, rue du Chevaleret
F-75013 Paris

Dr. Radu Ignat
Laboratoire de Mathematiques
Universite Paris Sud (Paris XI)
Batiment 425
F-91405 Orsay Cedex

Prof. Dr. Richard D. James
Dept. of Aerospace Eng. & Mechanics
University of Minnesota
110 Union Street S. E.
Minneapolis , MN 55455
USA

Dr. Bernd Kirchheim
Mathematisches Institut
Heinrich-Heine-Universität
Gebäude 25.22
Universitätsstr. 1
40225 Düsseldorf

Hans Knüpfer
Courant Institute of
Mathematical Sciences
New York University
251, Mercer Street
New York , NY 10012-1110
USA

Prof. Dr. Robert V. Kohn
Courant Institute of
Mathematical Sciences
New York University
251, Mercer Street
New York , NY 10012-1110
USA

Prof. Dr. Roman Kotecky
Center for Theoretical Study
Charles University
Jilska 1
110 00 Praha 1
CZECH REPUBLIC

Dr. Frederic Legoll
LAMI-ENPC
6 et 8 Avenue Blaise Pascal
Cite Descartes - Champs sur Marne
F-77455 Marne la Vallee Cedex 2

Prof. Dr. Stephan Luckhaus
Mathematisches Institut
Universität Leipzig
Johannisgasse 26
04103 Leipzig

Prof. Dr. Christof Melcher
Lehrstuhl I für Mathematik
RWTH Aachen
52056 Aachen

Dr. Carlos Mora-Corral
Basque Center for Applied Mathematics
Parque Tecnologico de Vizcaya
Edif. 500
E-48160 Derio (Vizcaya)

Prof. Dr. Stefan Müller
Haussdorf Center for Mathematics
& Institut für Angewandte Mathematik
Endenicher Allee 60
53115 Bonn

Benson K. Muite
Mathematical Institute
Oxford University
24-29 St. Giles
GB-Oxford OX1 3LB

Stefan Neukamm
Zentrum Mathematik
TU München
85747 Garching

Prof. Dr. Barbara Niethammer
Mathematical Institute
Oxford University
24-29 St. Giles
GB-Oxford OX1 3LB

Prof. Dr. Michael Ortiz
Division of Engineering and
Applied Sciences; MS 104-44
California Institute of Technology
Pasadena , CA 91125
USA

Dr. Christoph Ortner
Mathematical Institute
Oxford University
24-29 St. Giles
GB-Oxford OX1 3LB

Prof. Dr. Felix Otto
Institut für Angewandte Mathematik
Universität Bonn
Endenicher Allee 60
53115 Bonn

Prof. Dr. Oliver Penrose
Department of Mathematics
Heriot-Watt University
Riccarton
GB-Edinburgh EH 14 4AS

Prof. Dr. Antoni Planes
Departament ECM
Facultat de Fisica
Universitat de Barcelona
Diagonal 647
E-08028 Barcelona/Catalonia

Celia Reina Romo
Caltech
MS: 205-45
1200 E. California Blvd.
Pasadena CA 91125
USA

Prof. Dr. Ekhard K.H. Salje
Dept. of Earth Sciences
University of Cambridge
Downing Street
GB-Cambridge CB2 3EQ

Dr. Anja Schlömerkemper
Max-Planck-Institut für Mathematik
in den Naturwissenschaften
Inselstr. 22 - 26
04103 Leipzig

Dr. Bernd Schmidt
Zentrum Mathematik
Technische Universität München
85747 Garching bei München

Prof. Dr. Dominique Schryvers
Electron Microscopy for Materials
Research (EMAT)
Department of Physics, UA
Groenenborgerlaan 171
B-2020 Antwerp

Prof. Dr. Hanus Seiner
Institute of Thermomechanics
Academy of Sciences of Czech Republic
Dolejskova 5
18200 Praha 8
CZECH REPUBLIC

Prof. Dr. Angela Stevens
Universität Heidelberg
Angewandte Mathematik und Bioquant
Im Neuenheimer Feld 267
69120 Heidelberg

Prof. Dr. Endre Süli
Computing Laboratory
Oxford University
Wolfson Building
Parks Road
GB-Oxford OX1 3QD

Prof. Dr. Lev Truskinovsky
Laboratoire de Mecanique des
Solides
UMR-CNRS 7649
Ecole Polytechnique
F-91128 Palaiseau Cedex

Prof. Dr. Eric Vanden-Eijnden
Courant Institute of
Mathematical Sciences
New York University
251, Mercer Street
New York , NY 10012-1110
USA

Prof. Dr. Manfred Wuttig
Dept. of Chemical & Nuclear Eng.
University of Maryland
College Park , MD 20742-2111
USA

Barbara Zwicknagl
Hausdorff Center for Mathematics
Universität Bonn
Endenicher Allee 62
53115 Bonn